

THE HISTORY OF THE COSMIC SUPERNOVA RATE DERIVED FROM THE EVOLUTION OF THE HOST GALAXIES

CHIAKI KOBAYASHI¹, TAKUJI TSUJIMOTO², AND KEN'ICHI NOMOTO^{1,3}

¹ Department of Astronomy, School of Science, University of Tokyo, Bunkyo-ku, Tokyo 113-0033, Japan;
chiaki@astron.s.u-tokyo.ac.jp

² National Astronomical Observatory, Mitaka, Tokyo 181-8588, Japan; taku.tsujimoto@nao.ac.jp

³ Research Center for the Early Universe, School of Science, University of Tokyo, Bunkyo-ku, Tokyo 113-0033, Japan; nomoto@astron.s.u-tokyo.ac.jp

To be published in the Astrophysical Journal

ABSTRACT

We make a prediction of the cosmic supernova rate history as a composite of the supernova rates in spiral and elliptical galaxies. We include the metallicity effect on the evolution of Type Ia supernova (SN Ia) progenitors, and construct detailed models for the evolutions of spiral and elliptical galaxies in clusters and field to meet the latest observational constraints. In the cluster environment, the synthesized cosmic star formation rate (SFR) has an excess at $z \gtrsim 3$ corresponding to the early star burst in ellipticals and a shallower slope from the present to the peak at the redshift of $z \sim 1.4$ compared with Madau's plot. In the field environment, we assume that ellipticals form over a wide range of redshifts as $1 \lesssim z \lesssim 4$. The synthesized cosmic SFR has a broad peak around $z \sim 3$, which is in good agreement with the observed one. The resultant cosmic SFRs lead to the following predictions for the cosmic SN Ia rate: 1) The SN Ia rate in spirals has a break at $z \sim 2$ due to the low-metallicity inhibition of SNe Ia, regardless of clusters or field. 2) At high redshifts, the SN Ia rate has a strong peak around $z \sim 3$ in clusters, whereas in field much lower rate is expected, reflecting the difference in the formation epochs of ellipticals.

Subject headings: cosmology: theory — galaxies: abundances — galaxies: evolution — supernovae: general

1. INTRODUCTION

The search for high-redshift supernovae has been extensively conducted mainly to determine cosmological parameters by the Supernova Cosmology Project (Perlmutter et al. 1999) and the High- z Supernova Search Team (Schmidt et al. 1998). High-redshift supernovae can also provide useful information on the star formation history in the universe. Type Ia supernovae (SNe Ia) have been discovered up to $z \sim 1.32$ (Gilliland, Nugent & Phillips 1999), and the SN Ia rate has been estimated up to $z \sim 0.5$ (Pain et al. 1996; Pain 1999). With the Next Generation Space Telescope, both SNe Ia and Type II supernovae (SNe II) will be observed through $z \sim 4$. The SN II rate is directly connected with the star formation rate (SFR), and the SN Ia rate can also trace the SFR combined with a SN Ia progenitor model. In a theoretical approach, the cosmic SN Ia rate as a function of redshift has been constructed using the observed cosmic SFR (Ruiz-Lapuente & Canal 1998; Yungelson & Livio 1998, 2000; Sadat et al. 1998; Madau, Della Valle & Panagia 1998; Kobayashi et al. 1998, hereafter K98).

The cosmic SFR has been estimated observationally up to $z \sim 5$ from UV and H α luminosity densities with the help of spectral population synthesis models (e.g. Madau et al. 1996; Connolly et al. 1997). The observed cosmic SFR by Madau et al. (1996) shows a peak at $z \sim 1.4$ and a sharp decrease to the present. However, UV luminosities which are converted to the SFRs may be affected by the dust extinction (Pettini et al. 1998). Recent updates of the cosmic SFR show some different features (Tresse & Maddox 1998; Gronwall 1998; Treyer et al. 1998; Hughes et al. 1998; Glazebrook et al. 1999; Steidel et al. 1999),

one of which suggests that a peak lies around $z \sim 3$.

Among the several attempts to calculate the cosmic SN Ia rate using the observed cosmic SFR, K98 predicts that the cosmic SN Ia rate drops at $z \sim 1 - 2$, because the SN Ia occurrence depends on the metallicity. In their SN Ia progenitor model, the accreting white dwarf (WD) blows strong winds to reach the Chandrasekhar (Ch) mass limit (Hachisu, Kato & Nomoto 1996, 1999b). If the iron abundance of the progenitors is as low as $[\text{Fe}/\text{H}] \lesssim -1$, then the wind is too weak for SNe Ia to occur. This model successfully reproduces the observed chemical evolution of the solar neighborhood such as the evolution of the oxygen to iron ratio and the abundance distribution function of disk stars (K98).

Their finding that the occurrence of SNe Ia depends on the metallicity of the progenitor systems implies that the SN Ia rate strongly depends on the history of the star formation and metal-enrichment. The universe is composed of different morphological types of galaxies and therefore the cosmic SFR is a sum of the SFRs for different types of galaxies. As each morphological type has a unique star formation history, we should decompose the cosmic SFR into the SFR belonging to each type of galaxy and calculate the SN Ia rate for each type of galaxy.

In this paper, we first construct the detailed evolution models for different types of galaxies which are compatible with the stringent observational constraints, and apply them to reproduce the cosmic SFR for two different environments, i.e., clusters and field. Secondly we confirm that the metallicity-dependent SN Ia progenitor model, which has been already tested for the solar neighborhood, can explain the present supernova rates for all types of galax-

ies. Finally combining the above SN Ia model with the self-consistent galaxy models, we calculate the SN Ia rate history for each type of galaxy and predict the cosmic SN Ia rate as a function of redshift.

In the next section, we describe our computational method of the galaxy evolution with our SN Ia progenitor model. In section 3, we construct the star formation histories of spirals and ellipticals, and predict their supernova rate histories in section 4. In section 5, we make a prediction of the cosmic supernova rates as a composite of different types of galaxies in clusters and field. Discussion and conclusions are given in sections 6 and 7, respectively.

2. MODELS

2.1. Type Ia Supernova Model

The progenitors of the majority of SNe Ia are most likely the Ch mass WDs (e.g., Nomoto, Iwamoto & Kishimoto 1997a; Nomoto et al. 2000 for recent reviews), although the sub-Ch mass models might correspond to some peculiar subluminous SNe Ia. The early time spectra of the majority of SNe Ia are in excellent agreement with the synthetic spectra of the Ch mass models, while the spectra of the sub-Ch mass models are too blue to be compatible with observations (Höflich & Khokhlov 1996; Nugent et al. 1997). For the evolution of accreting WDs toward the Ch mass, two scenarios have been proposed: One is a double-degenerate (DD) scenario, i.e., merging of double C+O WDs with a combined mass surpassing the Ch mass limit (Iben & Tutukov 1984; Webbink 1984), and the other is a single-degenerate (SD) scenario, i.e., accretion of hydrogen-rich matter via mass transfer from a binary companion (e.g., Nomoto et al. 1994 for a review). The issue of DD versus SD is still debated (e.g., Branch et al. 1995 for a review), but theoretical modeling has indicated that the merging of WDs does not make typical SNe Ia (Saio & Nomoto 1985, 1998; Segretain, Chabrier & Mochkovitch 1997), and the lifetime of SNe Ia progenitors predicted by the DD scenario is too short to be compatible with the chemical evolution of the solar neighborhood (K98).

Our SD scenario has two progenitor systems: One is a red-giant (RG) companion with the initial mass of $M_{\text{RG},0} \sim 1M_{\odot}$ and an orbital period of tens to hundreds days (Hachisu et al. 1996, 1999ab). The other is a near main-sequence (MS) companion with an initial mass of $M_{\text{MS},0} \sim 2 - 3M_{\odot}$ and a period of several tenths of a day to several days (Li & van den Heuvel 1997; Hachisu et al. 1999a). In these progenitor systems, the C+O WD accretes H-rich matter from the companion star at a sufficiently high rate ($10^{-7} - 10^{-6}M_{\odot} \text{ yr}^{-1}$) to increase its mass to the Ch mass through steady hydrogen burning. With such a rapid accretion, the WD blows optically thick strong winds that play a key role in stabilizing the mass transfer and avoiding a common envelope formation.

The optically thick winds are driven by a strong peak of OPAL opacity at $\log T(\text{K}) \sim 5.2$ (e.g., Iglesias & Rogers 1993). Since the opacity peak is due to iron lines, the wind velocity v_w depends on the iron abundance $[\text{Fe}/\text{H}]$ (K98; Hachisu & Kato 2000), i.e., v_w is higher for larger $[\text{Fe}/\text{H}]$. The metallicity effect on SNe Ia is clearly demonstrated by the size of the regions to produce SNe Ia in the diagram of the initial orbital period versus initial mass of the companion star (see Fig.2 of K98). The SN Ia re-

gions are much smaller for lower metallicity because the wind becomes weaker. The wind velocity depends also on the luminosity L of the WD. The more massive WD has a higher L , thus blowing higher velocity winds (Hachisu et al. 1999b). In order for the wind velocity to exceed the escape velocity of the WD near the photosphere, the WD mass should be larger than a certain critical mass for a given $[\text{Fe}/\text{H}]$. This implies that the initial mass of the WD $M_{\text{WD},0}$ should already exceed that critical mass in order for the WD mass to grow to the Ch mass. This critical mass is larger for smaller $[\text{Fe}/\text{H}]$, reaching $1.1M_{\odot}$ for $[\text{Fe}/\text{H}] = -1.1$ (Fig.1 of K98). Here we should note that the relative number of WDs with $M_{\text{WD},0} \gtrsim 1.1M_{\odot}$ is quite small in close binary systems (Umeda et al. 1999). And for $M_{\text{WD},0} \gtrsim 1.2M_{\odot}$, the accretion leads to collapse rather than SNe Ia (Nomoto & Kondo 1991). Therefore, we assume that no SN Ia occur at $[\text{Fe}/\text{H}] \leq -1.1$ in our chemical evolution model.

The lifetimes of SNe Ia (i.e., the lifetimes of the binary systems from the formation through the explosion) are determined from the main-sequence lifetimes of the companion stars with the initial masses in the range $m_{d,\ell} \leq m \leq m_{d,u}$. In our chemical evolution model, we adopt $M_{\text{WD},0} = 1M_{\odot}$ and $Z = 0.004$ as a representative case. Then $m_{d,\ell} = 0.9M_{\odot}$ and $m_{d,u} = 1.5M_{\odot}$ for the RG+WD system and $m_{d,\ell} = 1.8M_{\odot}$ and $m_{d,u} = 2.6M_{\odot}$ for the MS+WD system, as seen in Figure 1 of K98. The distribution function of the companion stars (mass donors) is assumed to be $\phi_d(m) \propto m^{-x}$ with the slope of $x = 0.35$, and normalized to unity at $m_{d,\ell} \leq m \leq m_{d,u}$. This slope is determined from the distribution function of the initial mass of the companions which is taken from the observed mass ratio distribution in binaries (Duguennoy & Mayor 1991).

The progenitors of SNe Ia are assumed to have main sequence masses in the range of $m_{p,\ell} = 3M_{\odot}$ and $m_{p,u} = 8M_{\odot}$ and form C+O WDs. The total fraction of primary stars which eventually produce SNe Ia is denoted by b (see Eq.[12] in section 2.2 for the exact definition of b). The parameter b may depend on the binary fractions. If the binary fraction depends on the gas density in the star forming region, there should be a difference in b between spirals and ellipticals (we can expect the higher fraction for ellipticals). However the number of low-mass X-ray binaries per unit blue luminosity appears to be almost the same between spirals and ellipticals (Canizares, Fabiano & Trinchieri 1987; Matsushita et al. 1994), which means that the binary fraction does not depend on the gas density in the star-forming region. The parameter b may also depend on the metallicity. We have not included the metallicity dependence of the size of the SN Ia region. According to the simulations of Hachisu & Kato (2000), the area in the orbital period-companion mass plane does not increase with the metallicity for the MS+WD systems, but does increase for the RG+WD systems. Thus, only b for the RG+WD systems b_{RG} may be larger for higher metallicity. However there is no significant difference between the mean iron abundances of progenitors for the RG+WD systems in ellipticals and spirals. Thus, we determine the values of b to reproduce the chemical evolution in the solar neighborhood, and adopt the best-fit values for all types of galaxies. (We also show the results for other b

parameters in Appendix.) We search the parameter b with the χ^2 test for the $[\text{O}/\text{Fe}]$ - $[\text{Fe}/\text{H}]$ relation and the abundance distribution in the solar neighborhood, and get the allowed values of $0.04 \lesssim b_{\text{MS}} \lesssim 0.055$ for the MS+WD systems and $0.01 \lesssim b_{\text{RG}} \lesssim 0.04$ for the RG+WD systems under $2b_{\text{MS}} + b_{\text{RG}} \sim 0.12$. The best-fit values are $b_{\text{MS}} = 0.05$ and $b_{\text{RG}} = 0.02$ with the probability of more than $\sim 80\%$; the probability is as low as $\sim 65\%$ for $b_{\text{MS}} = b_{\text{RG}} = 0.04^1$ (see Appendix). The fraction of primary stars which eventually produce SNe Ia is given as functions of the companion's mass m_d and the companion's lifetime (i.e., lifetime of SNe Ia progenitor t_{Ia}) as

$$B_m(m_d) \equiv b \frac{1}{m_d} \phi_d(m_d) \left\{ \int_{m_{d,\ell}}^{m_{d,u}} \frac{1}{m} \phi_d(m) dm \right\}^{-1}, \quad (1)$$

$$B_t(t_{\text{Ia}}) \equiv B_m(m_d) \frac{dm_d}{dt_{\text{Ia}}}. \quad (2)$$

Figure 1 shows $B_m(m_d)$ (upper panel) and $B_t(t_{\text{Ia}})$ (lower panel) for the RG+WD and the MS+WD systems. In the lower panel, the solid and the dashed lines show the cases for $Z = 0.002$ and $Z = 0.02$ (solar), respectively.

In the one-zone uniform model for the chemical evolution of the solar neighborhood, the heavy elements in the metal-poor stars originate from the mixture of the SN II ejecta of various progenitor masses. The abundances averaged over the progenitor masses of SNe II predicts $[\text{O}/\text{Fe}] \sim 0.45$ (e.g., Tsujimoto et al. 1995; Nomoto et al. 1997b). Later SNe Ia start ejecting mostly Fe, so that $[\text{O}/\text{Fe}]$ decreases to ~ 0 around $[\text{Fe}/\text{H}] \sim 0$. The low-metallicity inhibition of SNe Ia predicts that the decrease in $[\text{O}/\text{Fe}]$ starts at $[\text{Fe}/\text{H}] \sim -1$. Such an evolution of $[\text{O}/\text{Fe}]$ well explains the observations (K98).

We should note that some anomalous stars have $[\text{O}/\text{Fe}] \sim 0$ at $[\text{Fe}/\text{H}] \lesssim -1$. The presence of such stars, however, is not in conflict with our SNe Ia models, but can be understood as follows: The formation of such anomalous stars (and the diversity of $[\text{O}/\text{Fe}]$ in general) indicates that the interstellar materials were not uniformly mixed but contaminated by only a few SNe II (or even single SN II) ejecta. This is because the timescale of mixing was longer than the time difference between the supernova event and the next generation star formation. The iron and oxygen abundances produced by a single SN II vary depending on the mass, energy, mass cut, and metallicity of the progenitor. Relatively smaller mass SNe II ($13\text{--}15M_\odot$) and higher explosion energies tend to produce $[\text{O}/\text{Fe}] \sim 0$ (Nomoto et al. 1997b; Umeda et al. 2000). Those metal poor stars with $[\text{O}/\text{Fe}] \sim 0$ may be born from the interstellar medium polluted by such SNe II.

The metallicity effect on SNe Ia can also be checked with the metallicity of the host galaxies of nearby SNe Ia. There has been no evidence that SNe Ia have occurred in galaxies with a metallicity of $[\text{Fe}/\text{H}] \lesssim -1$, although host galaxies are detected only for one third of SNe Ia and the estimated metallicities of host galaxies are uncertain. Three SNe Ia are observed in low-metallicity dwarf galaxies; SN1895B and SN1972E in NGC 5253, and SN1937C in IC 4182. Metallicities of these galaxies are estimated to be $[\text{O}/\text{H}] = -0.25$ and -0.35 , respectively (Kochanek 1997).

¹In K98, we adopt $b_{\text{MS}} = b_{\text{RG}} = 0.04$ which is determined from the Kolmogorov-Smirnov (KS) test.

If $[\text{O}/\text{Fe}] \sim 0$ as in the Magellanic Clouds, $[\text{Fe}/\text{H}] \sim -0.25$ and -0.35 which are not so small. Even if these galaxies have extremely SN II like abundance as $[\text{O}/\text{Fe}] \sim 0.45$, $[\text{Fe}/\text{H}] \sim -0.7$ and -0.8 (being higher than -1), respectively. Since these host galaxies are blue ($B - V = 0.44$ for NGC 5253 and $B - V = 0.37$ for IC 4182 according to RC3 catalog), the MS+WD systems are dominant progenitors for the present SNe Ia. The rate of SNe Ia originated from the MS+WD systems is not so sensitive to the metallicity as far as $[\text{Fe}/\text{H}] > -1$ (Hachisu & Kato 2000). Even if $[\text{Fe}/\text{H}] \sim -0.7$ in such blue galaxies, therefore, the SN Ia rate is predicted to be similar to those in more metal-rich galaxies.

Futhermore, our SN Ia model can well explain the diversity of SN Ia luminosity, by assuming that the more luminous SNe Ia are produced from smaller $M_{\text{WD},0}$ because of the larger C/O ratio. Observationally, the most luminous SNe Ia occur only in spirals, while both spirals and ellipticals are hosts for dimmer SNe Ia (Umeda et al. 1999). In our progenitor model, the WD with small $M_{\text{WD},0}$ ($\sim 0.7M_\odot$) can reach the Ch mass only when the companion stars is massive enough (i.e., t_{Ia} is short enough) to supply the necessary amount of mass ($\sim 0.7M_\odot$). Thus the brightest SNe Ia can occur only near the star forming region. The variation of the peak brightness of SNe Ia has been found to depend also on the location in the galaxy, i.e., the diversity decreases toward the outer regions of the galaxy (Wang, Höflich & Wheeler 1997). In our model, this trend is due to the metallicity gradient of the galaxy. In the outer region, the metallicity is so small that $M_{\text{WD},0}$ should be large enough to blow strong winds; thus only dim SNe Ia appear.

2.2. Galactic Evolution Model

A simplified model of the galactic chemical evolution is constructed with analytical equations (Tinsley 1980). The accretion of primordial gas from a reservoir in a halo is assumed to form a galaxy. By assuming that the accretion per time t (the infall rate R_{in}) is proportional to the mass of the reservoir, we get the exponential form of the infall rate with a infall timescale τ_i as

$$R_{\text{in}} = \frac{1}{\tau_i} \exp(-t/\tau_i). \quad (3)$$

Here we define the total baryon mass of the galaxy as the mass of the reservoir.

The gas fraction f_g is defined as the ratio of the gas mass in the bulge and disk to the total baryon mass of the galaxy (bulge, disk and halo), and Z_i is the mass fraction of a heavy element i in the gas. For ellipticals, the gas includes the gas ejected in the galactic wind. The SFR ψ is assumed to be proportional to the gas fraction (Schmidt 1959) as

$$\psi = \frac{1}{\tau_s} f_g, \quad (4)$$

where τ_s is the star formation timescale. Then the time variations of f_g and Z_i are given by the following equations:

$$\frac{df_g}{dt} = -\psi + E + E_{\text{Ia}} + R_{\text{in}}, \quad (5)$$

$$\frac{d(Z_i f_g)}{dt} = -Z_i \psi + E_{z_i} + E_{z_i, \text{II}} + E_{z_i, \text{Ia}} + Z_{i, \text{in}} R_{\text{in}}. \quad (6)$$

The metallicity Z is defined as the sum of Z_i from C to Zn. The initial conditions are $f_g = 0$ and $Z_i = 0$. The metallicity of the infall gas $Z_{i, \text{in}}$ is assumed to be 0.

From dying stars, gas is ejected into the interstellar medium by mass loss and SNe II at a rate of E and by SNe Ia at a rate of E_{Ia} . Heavy elements are ejected at a rate of E_{z_i} , $E_{z_i, \text{II}}$, and $E_{z_i, \text{Ia}}$ by mass loss, SNe II, and SNe Ia, respectively. These ejection rates are given by the following equations;

$$E = \int_{m_t}^{m_u} (1 - w_m) \psi(t - \tau_m) \phi(m) dm, \quad (7)$$

$$E_{z_i} = \int_{m_t}^{m_u} (1 - w_m - p_{z_i, m, \text{II}}) Z_i(t - \tau_m) \psi(t - \tau_m) \phi(m) dm, \quad (8)$$

$$E_{z_i, \text{II}} = \int_{m_t}^{m_u} p_{z_i, m, \text{II}} \psi(t - \tau_m) \phi(m) dm, \quad (9)$$

$$E_{\text{Ia}} = m_{\text{CO}} \mathcal{R}_{\text{Ia}}, \quad (10)$$

$$E_{z_i, \text{Ia}} = m_{\text{CO}} p_{z_i, m, \text{Ia}} \mathcal{R}_{\text{Ia}}. \quad (11)$$

Here $m_{\text{CO}} = 1.38 M_{\odot}$ is the white dwarf mass at the explosion. \mathcal{R}_{Ia} denotes the SN Ia rate, which is obtained as

$$\begin{aligned} \mathcal{R}_{\text{Ia}} = & b \int_{\max[m_{\text{p}, \ell}, m_t]}^{m_{\text{p}, u}} \frac{1}{m} \phi(m) dm \\ & \times \int_{\max[m_{\text{d}, \ell}, m_t]}^{m_{\text{d}, u}} \frac{1}{m} \psi(t - \tau_m) \phi_{\text{d}}(m) dm. \end{aligned} \quad (12)$$

As noted in section 2.1, our SN Ia scenario has two types of progenitors (i.e., the MS+WD and the RG+WD systems). We calculate the SN Ia rate for each binary with each b , $m_{\text{d}, \ell}$, and $m_{\text{d}, u}$, and combine them. The SN II rate \mathcal{R}_{II} is also obtained as

$$\mathcal{R}_{\text{II}} = \int_{\max[m_{\text{p}, u}, m_t]}^{m_u} \frac{1}{m} \psi(t - \tau_m) \phi(m) dm. \quad (13)$$

The lower mass limit for integrals is the turning off mass m_t at t which is the mass of the star with the main sequence lifetime $\tau_m = t$. τ_m is taken from Kodama & Arimoto (1997) as a function of metallicity Z . w_m is the remnant mass fraction, which is the mass fraction of a neutron star or a white dwarf. $p_{z_i, m, \text{II}}$ and $p_{z_i, m, \text{Ia}}$ are the stellar yields which are the mass fractions of newly produced and ejected heavy element i , which are given from the supernovae nucleosynthesis model (Tsujimoto et al. 1995; Nomoto et al. 1997b) with $p_{z_i, m, \text{II}} = 0$ for $m < 10 M_{\odot}$. We do not include the dependence of w_m , $p_{z_i, m, \text{II}}$ and $p_{z_i, m, \text{Ia}}$ on the stellar metallicity.

The initial mass function (IMF) is assumed to have time-invariant mass spectrum $\phi(m) \propto m^{-x}$ normalized to unity at $m_{\ell} \leq m \leq m_u$. Theoretical arguments indicate that the IMF originates from fragmentation of a gas cloud almost independently of local physics in the gas (Low & Lynden-Bell 1976; Silk 1977). A solar-neighborhood IMF would therefore be a good approximation, and we adopt the Salpeter slope of $x = 1.35$ (Salpeter 1955) and a mass

range from $m_{\ell} = 0.05 M_{\odot}$ to $m_u = 50 M_{\odot}$ (Tsujimoto et al. 1997).

The time variation of the stellar fraction f_s is calculated as

$$\frac{df_s}{dt} = \psi - E - E_{\text{Ia}}, \quad (14)$$

and the mean stellar metallicity $Z_{i, s}$ at the time t is obtained from the conservation of heavy elements;

$$Z_i f_g + Z_{i, s} f_s = \int_0^t \{E_{z_i, \text{II}} + E_{z_i, \text{Ia}} + Z_{i, \text{in}} R_{\text{in}}\} dt. \quad (15)$$

The photometric evolution of galaxies is calculated from the summation of the simple stellar population, which is defined as a single generation of coeval and chemically homogeneous stars of various masses, and taken from Kodama & Arimoto (1997) as a function of age t and metallicity Z . The passbands of photometric systems and the zero points are the same as Kodama & Arimoto (1997).

For a standard model, we adopt $H_0 = 50 \text{ km s}^{-1} \text{ Mpc}^{-1}$, $\Omega_0 = 0.2$, $\lambda_0 = 0$, and the galactic age of 15 Gyr, which corresponds to the redshift at the formation epoch of galaxies of $z_f \sim 4.5$.

3. STAR FORMATION HISTORIES OF GALAXIES

3.1. *Spiral Galaxies*

The star formation history can be inferred from the observed present-day colors of galaxies, by using the well-known technique of stellar population synthesis (Arimoto, Yoshii & Takahara 1992). In this paper, we determine the timescales τ_{I} and τ_{S} in equations (3) and (4) to reproduce both observed colors and gas fractions for four types of spirals, i.e., S0a-Sa, Sab-Sb, Sbc-Sc, and Scd-Sd. These values are summarized in Table 1. As shown in the top panel of Figure 2, earlier types of spirals form larger fractions of stars at an early epoch, thereby having redder and smaller gas fractions at present. The excellent agreements between models and the observations are shown in middle and bottom panels of Figure 2. The resultant present metallicities and colors are tabulated in Table 2. Observational data of the present $B - V$ colors for various types of spirals are taken from Roberts & Haynes (1994). We use the gas (i.e., HI+H₂) fractions which are normalized by the present blue luminosity of the galaxy to avoid the uncertainty in the fractions of the dark matter. The HI mass is taken from Roberts & Haynes (1994), and the H₂ mass is derived from the H₂/HI ratios (Casoli et al. 1998).

3.2. *Elliptical Galaxies*

The star formation history in elliptical galaxies is still controversial, with single star burst models on one hand and continuous star formation models at the other extreme. In the former, elliptical galaxies are formed through dissipative collapse of a protogalactic cloud with a single star burst at a very early epoch (e.g., Larson 1974; Arimoto & Yoshii 1987; Kodama & Arimoto 1997). In the latter, elliptical galaxies grow through mergers of gaseous galaxies with a continuous star formation through later epoch (e.g., Kauffmann & Charlot 1998; Baugh et al. 1998).

The dissipative collapse scenario assumes that the star formation in ellipticals has stopped by a loss of gases due to

a supernova-driven galactic wind (Larson 1974; Arimoto & Yoshii 1987), so that the bulk of the stars are old and have formed at $z \gtrsim 2$. The galactic wind model can well reproduce the passive evolution of colors observed in cluster ellipticals (Stanford, Eisenhardt & Dickinson 1998; Kodama & Arimoto 1997). On the other hand, the semi-analytical simulations of hierarchical clustering (Kauffmann & Charlot 1998; Baugh et al. 1998) based on the cold dark matter (CDM) scenario suggest that the formation of ellipticals are protracted toward lower redshifts especially in the low-density region such as present-day field. Such environmental effect is imprinted in the morphology-density relation (Dressler 1980; Dressler et al. 1997). There are some observational evidences that not all field ellipticals are as old as cluster ellipticals (Zepf 1997; Franceschini et al. 1998; Kodama, Bower & Bell 1999). However the relation of Mg_2 indices and velocity dispersions implies the age difference of only ~ 1 Gyr among cluster, group and field ellipticals (Bernardi et al. 1998).

Taking into account the possibility that there exists the environmental effect on the galaxy formation, we set two models for ellipticals in clusters and field, respectively.

1) For cluster ellipticals, we adopt the galactic wind model. The epoch of galactic wind t_{gw} (i.e., the epoch of the end of star formation) is determined from the dynamical potential of the galaxy (Larson 1974), and we assume $t_{\text{gw}} = 1$ Gyr on the average which corresponds to the redshift of $z \sim 3$. The adopted τ_i and τ_s in equations (3) and (4) are summarized in Table 1, and the resultant present metallicities and colors are in Table 2. This star formation history is constructed to reproduce the observational constraints such as the present mean stellar metallicity of $Z_s \sim 0.6Z_\odot$ averaged over the whole galaxy (Kobayashi & Arimoto 1999), the present $B - V$ color (Roberts & Haynes 1994), and the color evolution observed at $0 \lesssim z \lesssim 1$ as shown in Figure 3a. The circles, triangles, and crosses show the average differences in the observed colors of cluster galaxies at each redshifts relative to the same rest-frame colors of Coma E+S0 galaxies (Stanford, Eisenhardt & Dickinson 1998). Thus, no color difference represents no evolution relative to Coma. The observed color differences are as small as our model prediction, which means that ellipticals have evolved passively from $z \sim 1$. In this model, the duration of the star formation is short enough to be consistent with the observational estimates of the magnesium to iron ratio $[Mg/Fe] \sim 0.3$ (Worthey, Faver & Gonzalez 1992; Kobayashi & Arimoto 1999).

2) For field ellipticals, we adopt the same star formation history as in cluster ellipticals, and assume that the formation epochs span a wide range of redshifts. The distribution function of the formation epoch ϕ_{z_f} is assumed as

$$\phi_{z_f} \propto \frac{1}{3} \left(z - \frac{2\sqrt{3}}{\sqrt{3}-1} \right)^3 - \left(\frac{2}{\sqrt{3}-1} \right)^2 \left(z - \frac{2\sqrt{3}}{\sqrt{3}-1} \right), \quad (16)$$

which gives $\phi_{z_f} = 0$ at $z = 0$ and $\frac{d\phi_{z_f}}{dz} = 0$ at $z = 2$, and is normalized to unity at $0 \leq z \leq z_f$. As shown in Figure 3b, this formulation can meet the distribution function of z_f which is derived from the observational estimates of z_f for 34 field ellipticals in the Hubble Deep Field, using the broadband spectra (Franceschini et al. 1998).

4. SUPERNOVA RATES IN GALAXIES

Present supernova rates observed in the various types of galaxies (Cappellaro et al. 1997; Cappellaro, Evans & Turatto 1999) put the constraints on the SN Ia progenitor models. Using the galaxy models in section 3, we show that our SN Ia model can well reproduce the present supernova rates in both spirals and ellipticals.

4.1. *Spiral Galaxies*

The observed SN II rate \mathcal{R}_{II} in late-type spirals is about twice the rate in early-type spirals. On the other hand, the observed SN Ia rates \mathcal{R}_{Ia} in both types of spirals are nearly the same. Thus the present $\mathcal{R}_{\text{Ia}}/\mathcal{R}_{\text{II}}$ ratio in early-type spirals is larger than that in late-type spirals by a factor of ~ 2 . Such a difference in the relative frequency is a result of the difference in the SFR (see section 3.1), because the different dependences of \mathcal{R}_{II} and \mathcal{R}_{Ia} on the SFR are due to the different lifetimes of supernova progenitors. Therefore the observed $\mathcal{R}_{\text{Ia}}/\mathcal{R}_{\text{II}}$ ratio gives a constraint on the SN Ia progenitor model.

Figure 4 shows the predicted evolutionary change in $\mathcal{R}_{\text{Ia}}/\mathcal{R}_{\text{II}}$ ratios for early and late types of spirals, compared with the observations. The solid, dashed, and dotted lines show the results for our SN Ia model, the single delay-time model with $t_{\text{Ia}} \sim 1.5$ Gyr (Yoshii, Tsujimoto & Nomoto 1996), and the DD model (Tutukov & Yungelson 1994), respectively. In the DD model, the lifetime of majority of SNe Ia is $\sim 0.1 - 0.3$ Gyr, so that the evolution of \mathcal{R}_{Ia} is similar to \mathcal{R}_{II} . Therefore $\mathcal{R}_{\text{Ia}}/\mathcal{R}_{\text{II}}$ is insensitive to the SFR. This results in the small differences in $\mathcal{R}_{\text{Ia}}/\mathcal{R}_{\text{II}}$ among the various type of spirals, which is not consistent with observations. For the similar reason, the single delay-time model with $t_{\text{Ia}} \sim 1.5$ Gyr is not acceptable.

In our SN Ia model, if the iron abundance of progenitors is $[Fe/H] \gtrsim -1$, the occurrence of SNe Ia is determined from the lifetime of the companions, which is $t_{\text{Ia}} \sim 0.5 - 1.5$ Gyr for the MS companions and $\sim 2 - 20$ Gyr for the RG companions (see Fig.1). If SNe Ia occurred only in the MS+WD systems with relatively short lifetimes, $\mathcal{R}_{\text{Ia}}/\mathcal{R}_{\text{II}}$ would have been insensitive to the SFR. On the contrary, if SNe Ia occurred only in the RG+WD systems with longer lifetimes, the present difference in $\mathcal{R}_{\text{Ia}}/\mathcal{R}_{\text{II}}$ between early and late type spirals would have been too large, reflecting the large difference in SFR at an early epoch. Owing to the presence of these two kinds of the progenitor systems in our SN Ia progenitor model, the observed difference in $\mathcal{R}_{\text{Ia}}/\mathcal{R}_{\text{II}}$ can be reproduced. We note that the present SN Ia rate depends on the b parameters, especially b_{RG} (see Appendix for more details).

4.2. *Elliptical Galaxies*

Figure 5 shows the SN Ia rate history in ellipticals. As noted in section 3.2, we assume that the bulk of stars in cluster ellipticals are formed at $z \gtrsim 3$ and have ages older than 10 Gyr. Thus, in the single delay-time model (dashed line) and the DD model (dotted line), the SN Ia lifetimes are too short to reproduce the observed SN Ia rate at the present epoch. In ellipticals, the chemical enrichment takes place so early (see Fig.7b) that the metallicity effect on SN Ia is not effective, and therefore the SN Ia rate depends almost only on the lifetime. Our SN

Ia model (solid line) includes the RG+WD systems with $t_{\text{Ia}} \gtrsim 10$ Gyr, thus well reproducing the present SN Ia rate in ellipticals.

A burst of SNe Ia occur after ~ 0.5 Gyr from the beginning of the star formation, because SNe Ia start to occur from the MS+WD systems at their shortest lifetime. The second peak of the SN Ia rate appears after ~ 2 Gyr, because of the onset of SNe Ia from the RG+WD systems. If we apply the age-redshift relation in Figure 5, these two peaks appear at $z \sim 2.5$ and ~ 1.5 , respectively. From $z \sim 0.2$ to $z \sim 0$, the SN Ia rate gradually decreases by $\sim 40\%$. Majority of SN Ia progenitors with $Z = 0.002$ have already exploded at $z < 0.2$ and only more metal-rich SNe Ia occur at $z \sim 0$. This is because the lifetime τ_m of the smallest mass companions ($0.9M_{\odot}$) depends on the metallicity as $\tau_m \sim 11$ Gyr for $Z = 0.002$ and $\tau_m \sim 19$ Gyr for $Z = 0.02$ (see Fig.1).

The decrease in the SN Ia rate from $z \sim 0.2$ to $z \sim 0$ depends also on the star formation history in ellipticals and the galactic age. If we adopt the galactic age of 12 Gyr, such a decrease in the SN Ia rate does not appear. If ellipticals have undergone the relatively continuous star formation, as suggested by the hierarchical clustering simulations, the SN Ia rate might keep constant to the present. The predicted rate for $H_0 = 50 \text{ km s}^{-1} \text{ Mpc}^{-1}$ adopted in our calculation is a little higher than the observations at present. We can get better fit for $H_0 = 65 \text{ km s}^{-1} \text{ Mpc}^{-1}$, because the absolute value in our model is independent of the cosmological parameters, while the observed SN Ia rate is proportional to H_0^2 . The present SN Ia rate also depends on the b parameter, especially b_{RG} (see Appendix for more details).

5. COSMIC SUPERNOVA RATE

Galaxies that are responsible for the cosmic SFR have different timescales for the heavy-element enrichment, and the occurrence of supernovae depends on the metallicity therein. Therefore we calculate the cosmic supernova rate by summing up the supernova rates in spirals and ellipticals with the ratio of the relative mass contribution. The relative mass contribution of i -th type of galaxies is obtained from the observed relative luminosity proportion $c_i = 0.215, 0.185, 0.160, 0.275$, and 0.165 (Pence 1976) for ellipticals, S0a-Sa, Sab-Sb, Sbc-Sc, and Scd-Sd, respectively, and the calculated mass to light ratio in B-band $(M/L_B)_i$ for each galaxy model, as given in Table 2.

To compare the observed cosmic SFR, we convert the predicted cosmic SFR per mass to the cosmic SFR per volume by multiplying a constant ($\rho_c \Omega_{\text{g}\infty}$) as follows;

$$\psi_{\text{cosmic}} [M_{\odot} \text{yr}^{-1} \text{Mpc}^{-3}] = \rho_c \Omega_{\text{g}\infty} \frac{\sum_i c_i (M/L_B)_i \psi_i [\text{Gyr}^{-1}]}{\sum_i c_i (M/L_B)_i}. \quad (17)$$

Here ρ_c is the critical density in the cosmology ($\rho_c = \frac{3c^2}{8\pi G} H_0^2$) and $\Omega_{\text{g}\infty}$ is the initial comoving density of the gas defined by Pei & Fall (1995). $\Omega_{\text{g}\infty}$ is constrained from the stellar comoving density at present. The gas and stellar comoving densities are given by

$$\Omega_{\text{g}} = \Omega_{\text{g}\infty} \frac{\sum_i c_i (M/L_B)_i f_{\text{g},i}}{\sum_i c_i (M/L_B)_i}, \quad (18)$$

$$\Omega_{\text{s}} = \Omega_{\text{g}\infty} \frac{\sum_i c_i (M/L_B)_i f_{\text{s},i}}{\sum_i c_i (M/L_B)_i}. \quad (19)$$

We adopt $\Omega_{\text{g}\infty} = 3.5 \times 10^{-3} h^{-1}$ to reproduce the present stellar comoving density $\log \Omega_{\text{s}0} = -2.3$ (Fukugita, Hogan & Peebles 1998), which gives the present gas comoving density of $\log \Omega_{\text{g}0} = -3.6$.

The cosmic SN II or Ia rate \mathcal{R}_{SN} per luminosity and per volume are given as

$$\mathcal{R}_{\text{SN,cosmic}} [(10^{10} L_{B\odot})^{-1} \text{Century}^{-1}] = \frac{\sum_i c_i \mathcal{R}_{\text{SN},i} [(10^{10} L_{B\odot})^{-1} \text{Century}^{-1}]}{\sum_i c_i} \quad (20)$$

$$\mathcal{R}_{\text{SN,cosmic}} [\text{yr}^{-1} \text{Mpc}^{-3}] = \rho_c \Omega_{\text{g}\infty} \frac{\sum_i c_i (M/L_B)_i \mathcal{R}_{\text{SN},i} [M_{\odot}^{-1} \text{Gyr}^{-1}]}{\sum_i c_i (M/L_B)_i} \quad (21)$$

If we adopt larger $\Omega_{\text{g}\infty}$, we get larger $\Omega_{\text{s}0}$ and thus larger ψ_{cosmic} . However, the $\mathcal{R}_{\text{SN,cosmic}}$ per luminosity does not depend on $\Omega_{\text{g}\infty}$.

5.1. In Clusters

First, we make a prediction of the cosmic supernova rates in cluster galaxies. We use the galaxy models which are in good agreements with the observational constraints as shown in Figures 2 and 3. Figure 6a shows the cosmic SFR along redshift (solid line) as a composite of those in spirals (long-dashed line) and ellipticals (short-dashed line). In our galaxy models, ellipticals undergo a star burst at $z \gtrsim 3$ and the duration of the star formation is ~ 1 Gyr, while spirals undergo relatively continuous star formation. Thus, only the SFR in spirals is responsible for the cosmic SFR at $z \lesssim 2$. For comparison, the observed cosmic SFR in field, so-called Madau's plot (Gallego et al. 1995; Lilly et al. 1996; Madau et al. 1996; Connolly et al. 1997), is also plotted. Compared with Madau's plot, the predicted slope from the present to the peak at $z \sim 1.4$ is a little shallower (see also Totani, Yoshii & Sato 1997). Also the predicted peak of the SFR in ellipticals at $z \gtrsim 3$ is not seen in Madau's plot.

Possible sources of these differences between the theoretical SFR and observational data might be as follows; 1) Observational uncertainties: Recent observations have revealed the controversial situation, i.e., the slope of the SFR from $z \sim 0$ to $z \sim 1$ is much shallower than the Madau's plot according to Tresse & Maddox (1998), Treyer et al. (1998), and Gronwall (1998), while it is steeper according to Rowan-Robinson et al. (1997) and Glazebrook et al. (1999). Also the SFR is higher than Madau's plot at $z \gtrsim 2$ (Hughes et al. 1998; Pettini et al. 1998) and continues to be high toward $z \sim 5$ (Steidel et al. 1999). 2) The star formation at $z \gtrsim 3$ may be hidden by the dust extinction (Pettini et al. 1998). 3) Ellipticals may have formed at $z \sim 5$ (Totani et al. 1997). We here propose one more possibility: 4) The theoretical model is constructed for cluster galaxies, while the observational data are taken from field galaxies. Then these rates can be different, if the star formation histories depends on their environment. The cosmic SFR histories in field is much less clear than in clusters.

Figure 6b shows the cosmic supernova rates (solid line) as a composite of those in spirals (long-dashed line) and ellipticals (short-dashed line). The upper and lower three lines show the SN II and Ia rates, respectively. Our SN

Ia model is in good agreement with the observed rate at $z \sim 0.5$ (Pain et al. 1996; Pain 1999); here the number of sample has been increased from 3 SNe Ia in Pain et al. (1994) to 38 SNe Ia in Pain (1999), so that the errorbar has been greatly reduced. As we will observe supernovae at higher and higher redshift, the SN Ia rates are predicted to sharply decrease at certain redshifts, which we denote as $z_{\text{Ia,s}}$, $z_{\text{Ia,e}}$, and $z_{\text{Ia,tot}}$ for in spirals, ellipticals, and all types of galaxies (spirals plus ellipticals), respectively.

The SN Ia rate in spirals drops at $z_{\text{Ia,s}} \sim 1.9$ because of the low-metallicity inhibition of SNe Ia. We can test the metallicity effect by finding this drop of the SN Ia rate in spirals, if high-redshift SNe Ia at $z \gtrsim 1.5$ and their host galaxies are observed with the Next Generation Space Telescope.

In ellipticals, the chemical enrichment takes place so early that the metallicity is large enough to produce SNe Ia at $z \gtrsim 2$. Since we assume that the formation epoch of ellipticals is $z_f \sim 4.5$, the SN Ia rate in ellipticals decreases at $z_{\text{Ia,e}} \sim 2.6$. This redshift is determined from the shortest lifetime of SNe Ia, which is ~ 0.5 Gyr in our model (Fig.1). We should note that $z_{\text{Ia,e}}$ depends on the formation epoch of ellipticals, which is constrained from the color-magnitude relation in the cluster elliptical galaxies at $z \gtrsim 3$ (Kodama & Arimoto 1997). The two peaks of SN Ia rates at $z \sim 2.5$ and $z \sim 1.5$ come from the MS+WD and the RG+WD systems, respectively (see section 4.2). Between these peaks, the SN Ia rate decreases at $z_{\text{Ia,e}} \sim 1.6$. (Note, however, this drop disappears if we adopt $z_f \sim 3$, because the peak from the MS+WD systems moves to lower redshifts.) At $z \gtrsim 2.5$, the total SN Ia rate decreases as ellipticals at $z_{\text{Ia,tot}} \sim 2.6$. At $z \lesssim 2$, the total SN Ia rate decreases as spirals at $z_{\text{Ia,tot}} \sim 1.9$, because the contribution of ellipticals in the total SN Ia rate is smaller than spirals. However, the contribution of ellipticals can be larger depending on b (see Appendix). Figure 6c is the same as Figure 6b, but for the supernova rate per volume.

These redshifts, $z_{\text{Ia,s}}$, $z_{\text{Ia,e}}$ and $z_{\text{Ia,tot}}$, depend on the speed of the chemical enrichment in the host galaxies. Figure 7b shows the evolution of the iron abundance of gases in spirals (long-dashed line) and ellipticals (short-dashed line). For ellipticals, the model line is truncated at $z = 3.05$, where ellipticals lose their gases by the galactic wind. As the chemical enrichment in ellipticals takes place in short time, the iron abundance reaches $[\text{Fe}/\text{H}] \sim -1$ at $z \sim 4.3$. Then, the low metallicity effect on SNe Ia does not appear. In spirals, the iron abundance reaches $[\text{Fe}/\text{H}] \sim -1$ later at $z \sim 2.3$, which results in the drop of the SN Ia rate at $z_{\text{Ia,s}} \sim 1.9$.

For comparison, we calculate the cosmic supernova rates for the cosmic SFR constructed by connecting the the observational data (Fig.7a). In Figure 7a, the solid line (and the dotted line) is obtained with (and without) taking into account a correction of the dust extinction (Pettini et al. 1998). The initial gas comoving density is assumed to be $\Omega_{\text{g}\infty} = 3.2 \times 10^{-3} h^{-1}$. The adopted cosmic SFR increases from the H α data point at $z = 0$ (Gallego et al. 1995), makes a peak at $z \sim 1.4$, and decreases towards higher redshifts. It goes through the HDF UV data points which take into account a correction of the dust extinction (Pet-

tini et al. 1998). The corresponding cosmic chemical evolution is shown by the dotted line in Figure 7a. Because of the lower SFR than in Figure 6a at high redshifts, $[\text{Fe}/\text{H}] \sim -1$ is reached at smaller redshift and the total SN Ia rate decreases at $z_{\text{Ia,tot}} \sim 1.6^2$.

5.2. In the Field

We also predict the cosmic supernova rates assuming that the formation of ellipticals in fields took place for over the wide range of redshifts (Fig.3b). Figure 8a shows the cosmic SFR along redshift (solid line) as a composite of those in spirals (long-dashed line) and field ellipticals (short-dashed line). The SFR in spirals is the same as Figure 6a, but the star formation in ellipticals continues up to the present. Although the timescale of star formation in each elliptical is as short as in Figure 6a, the SFR averaged over the field ellipticals gradually increases toward higher redshifts. This is because the formation epochs of the field ellipticals distribute as in Figure 3b. The synthesized cosmic SFR is in good agreement with the observed one, except for the recent H α data at $z \sim 0.9$ (Glazebrook et al. 1999). The peak of the star formation appears at $z \sim 3$, which is consistent with the recent sub-mm data (Hughes et al. 1998).

Figure 8b shows the cosmic supernova rates (solid line) as a composite of those in spirals (long-dashed line) and ellipticals (short-dashed line). The upper and lower lines show the SN II and Ia rates, respectively. As in Figure 6b, the SN Ia rate in spirals drops at $z_{\text{Ia,s}} \sim 1.9$. The averaged SN Ia rate in ellipticals decreases at $z_{\text{Ia,e}} \sim 2.2$ as a result of ~ 0.5 Gyr delay of the decrease in the SFR at $z \gtrsim 3$. (We should note that $z_{\text{Ia,e}}$ depends on the distribution function of the formation epochs in Figure 3b, which is still uncertain.) Then, the total SN Ia rate decreases gradually from $z_{\text{Ia,tot}} \sim 2$ to $z \sim 3$. However, the contribution of ellipticals can be larger depending on b (see Appendix). Figure 8c is the same as Figure 8b but for the supernova rate per volume.

The rate of SNe II in ellipticals evolves following the SFR without time delay. Then, it is possible to observe SNe II in ellipticals around $z \sim 1$. The difference in the SN II and Ia rates between cluster and field ellipticals reflects the difference in the galaxy formation histories in the different environments.

6. DISCUSSION

We have made predictions in Figures 6b and 8b that the SN Ia rates have breaks at $z_{\text{Ia,s}}$, $z_{\text{Ia,e}}$, and $z_{\text{Ia,tot}}$ in spirals, ellipticals, and all types of galaxies, respectively. The exact values of the break redshifts depend on still uncertain factors. Here we discuss these dependences and uncertainties in order to know what we can learn when the Next Generation Space Telescope will obtain these redshifts.

6.1. SN Ia Rates in Spiral Galaxies

For spirals, $z_{\text{Ia,s}}$ corresponds to the point where the metallicity reaches $[\text{Fe}/\text{H}] \sim -1$. Therefore $z_{\text{Ia,s}}$ is determined by the $Z - z$ relation (metallicity-redshift relation), which involves the uncertainties in the $t - Z$ relation (age-metallicity relation) and the $t - z$ relation (time-redshift

²In the model in Figure 4 of K98, $z_{\text{Ia,tot}}$ is as small as ~ 1.2 , because the dust correction was not included (like the dotted line in Fig.7a) and $\Omega_{\text{g}\infty} = 2 \times 10^{-3} h^{-1}$ was adopted.

relation). Note the $t - z$ relation in galaxies depends not only on the cosmological model but also on the formation epoch of the galaxies z_f .

Among the above factors, the uncertainty in modeling the evolution of spiral galaxies is relatively small. The standard evolution model for spiral galaxies has been obtained by constructing the detailed model for the Galaxy which has a number of observational constraints. Based on the parameters on the IMF and the SN Ia rate determined for the Galaxy, we have developed the models for other types of spiral galaxies. Furthermore, the parameters on the SFR have been constrained from the gas fractions and colors of present-day spirals as in Figure 2.

As for the $t - z$ relation, a set of the cosmological parameters (H_0 , Ω_0 , λ_0) and z_f are constrained from the Galactic age which settles down to $\sim 12 - 15$ Gyr from the recent *HIPPARCOS* data (Gratton et al. 1997; Harris et al. 1997). (Here we assume the same z_f for all types of spirals.) In our calculations, we adopt $(H_0, \Omega_0, \lambda_0) = (50, 0.2, 0)$ that gives the cosmological age of ~ 16.5 Gyr and thus allows the galactic age of $t_{\text{gal}} = 15$ Gyr; these parameters lead to $z_{\text{Ia,s}} \sim 1.9$. If we adopt $(H_0, \Omega_0, \lambda_0) = (50, 1.0, 0)$ and $(65, 0.2, 0)$, which give shorter cosmological ages and allows the galactic age of $t_{\text{age}} = 12$ Gyr, we obtain smaller values of $z_{\text{Ia,s}} \sim 1.3$ and 1.8, respectively. On the other hand, the Λ -dominant model, e.g., $(H_0, \Omega_0, \lambda_0) = (65, 0.2, 0.8)$ with the galactic age of $t_{\text{age}} = 15$ Gyr, predicts $z_{\text{Ia,s}} \sim 2.1$. The uncertainty in the $t - z$ relation therefore results in $1.5 \lesssim z_{\text{Ia,s}} \lesssim 2$. The uncertainty from the $t - Z$ relation is smaller.

6.2. SN Ia Rates in Elliptical Galaxies

For cluster ellipticals, the uncertainty in the $t - Z$ relation is much smaller than spirals, because $[\text{Fe}/\text{H}]$ reaches ~ -1 in several 10^8 years by the star burst. The parameters for SFR is constrained from the color evolution of the cluster ellipticals, although other star formation histories may be allowed for the field ellipticals.

Like $z_{\text{Ia,s}}$, the $t - z$ relation affects $z_{\text{Ia,e}}$. Especially a large uncertainty lies in z_f . In our calculations, we assume $z_f \sim 4.5$ and it results in the decrease of the SN Ia rate twice at $z_{\text{Ia,e}} \sim 1.6$ and ~ 2.6 , which respectively correspond to the lifetimes of the MS+WD and the RG+WD systems after z_f (Fig.6b). However, the observational constraint from the color evolution on z_f only requires $z_f \gtrsim 3$ for cluster ellipticals. With other cosmological models and z_f , the uncertainty in the $t - z$ relation results in $z_{\text{Ia,e}} \gtrsim 2$ and $1 \lesssim z_{\text{Ia,e}} \lesssim 2$ for the MS+WD and the RG+WD systems, respectively.

For field ellipticals, there are large uncertainties in both $t - z$ and $t - Z$ relations owing to little information from observations, including the possibility that there is little difference between cluster and field ellipticals. To discuss quantitatively the uncertainties in $z_{\text{Ia,e}}$ in field, further observational information would be needed.

6.3. Total SN Ia Rates

If the many of the host galaxy types are not identified, the total rate of the spirals and elliptical components would depend on the parameters in more complicated manner.

In Figure 6b, the first break of the total SN Ia rate ap-

pears clearly at $z_{\text{Ia,tot}} \sim 1.9$. This is the case if $z_f \sim 4.5$ and the contribution of ellipticals ($z_{\text{Ia,e}} \sim 1.6$) is smaller than spirals ($z_{\text{Ia,s}} \sim 1.9$). If $z_f \sim 3$, for example, the break at $z_{\text{Ia,tot}} \sim 1.9$ disappears. The second break at $z_{\text{Ia,tot}} \sim 2.6$ corresponds to the second $z_{\text{Ia,e}}$.

Furthermore the ambiguity in the relative mass fractions c_i of spirals and ellipticals makes a prediction of the first $z_{\text{Ia,tot}}$ more complicated, while the second one remains unchanged. If the relative contribution from ellipticals is larger, the first $z_{\text{Ia,tot}}$ appears at the first $z_{\text{Ia,e}}$ (e.g., $z \sim 1.6$ for $z_f \sim 4.5$). Besides in our calculations the relative mass fractions c_i of galaxies are assumed to be constant against the redshift. If there is the number evolution of galaxies as suggested by the hierarchical clustering scenario, the star formation history and thus the supernova rate in ellipticals are similar to those for field ellipticals.

7. CONCLUSIONS

We have made predictions of the cosmic supernova rate history as a composite of the supernova rates in different types of galaxies. We adopt the SN Ia progenitor scenario including the metallicity effect which successfully reproduces the chemical evolution of the solar neighborhood (K98). We construct the evolution models for spiral and elliptical galaxies to meet the latest observational constraints such as the present gas fractions and colors for spirals, and the mean stellar metallicity and the color evolution from the present to $z \sim 1$ for ellipticals.

Owing to the presence of the *two* kinds of the SN Ia progenitor systems (MS+WD and RG+WD) with shorter (0.5 – 1.5 Gyr) and longer lifetimes (2 – 20 Gyr), respectively, we can explain the difference in the relative ratio of the SN Ia to SN II rate $\mathcal{R}_{\text{Ia}}/\mathcal{R}_{\text{II}}$ between early and late types of spirals. Owing to the presence of the RG+WD systems with over 10 Gyr lifetime, SNe Ia can be seen even at present in ellipticals where the star formation has already ceased more than 10 Gyr before.

We then construct the cosmic SFR as a composite of the SFRs for different types of galaxies, and predict the cosmic supernova rates for two different environments:

1. In the cluster environment, the synthesized cosmic SFR has an excess at $z \gtrsim 3$ due to the early star burst in ellipticals and a shallower slope from the present to the peak at $z \sim 1.4$, compared with Madau's plot. The predicted cosmic supernova rate suggests that in ellipticals SNe Ia can be observed even at high redshifts because the chemical enrichment takes place so early that the metallicity is large enough to produce SNe Ia at $z \gtrsim 2.5$. In spirals the SN Ia rate drops at $z \sim 2$ because of the low-metallicity inhibition of SNe Ia.
2. In the field environment, ellipticals are assumed to form at such a wide range of redshifts as $1 \lesssim z \lesssim 4$. The synthesized cosmic SFR has a broad peak around $z \sim 3$, which is in good agreement with the recent sub-mm observation by Hughes et al. (1998). The SN Ia rate is expected to be significantly low beyond $z \gtrsim 2$ because the SN Ia rate drops at $z \sim 2$ in spirals and gradually decreases from $z \sim 2$ in ellipticals.

This work has been supported in part by the grant-in-Aid for Scientific Research (08640336) and COE research (07CE2002) of the Ministry of Education, Science, Culture, and Sports in Japan. C.K. thanks to the Japan Society for Promotion of Science for a financial support. K.N. thanks to the participants in the workshop on “Type Ia Su-

pernova” (Aspen Center for Physics, 13-24 June 1999) for informative discussion. We would like to thank I. Hachisu and M. Kato for providing us with their new results, B. Schmidt for fruitful discussions, and T. Kodama for providing us with the database of simple stellar population spectra.

APPENDIX

B PARAMETER DEPENDENCE

Present supernova rates

The SN Ia rate prediction involves some uncertainties associated with the SN Ia progenitor model, which are mostly reflected in the uncertainty in b parameters given in section 2.1. b_{MS} and b_{RG} are the parameters for the total fraction of the WDs (with the initial mass of $3 - 8M_{\odot}$) which eventually produce SNe Ia in the MS+WD and the RG+WD systems, respectively (see Eq.[12] in section 2.2 for the exact definition of b). In the present study, the parameter set of [$b_{\text{MS}} = 0.02, b_{\text{RG}} = 0.05$] is chosen to best reproduce the chemical evolution in the solar neighborhood. Other sets of b parameters can also be approximately consistent with the chemical evolutions, but provide different predictions of the present supernova rates as follows.

a) *supernova rates in spiral galaxies* — In Figure 4, we use the relative ratio of the present SN Ia to SN II rates $\mathcal{R}_{\text{Ia}}/\mathcal{R}_{\text{II}}$ to avoid the H_0 uncertainty included in the observed supernova rates. The adopted set of [$b_{\text{MS}} = 0.02, b_{\text{RG}} = 0.05$] is seen to give also the best fit to $\mathcal{R}_{\text{Ia}}/\mathcal{R}_{\text{II}}$. If we adopt larger b_{RG} , $\mathcal{R}_{\text{Ia}}/\mathcal{R}_{\text{II}}$ is larger. For [$b_{\text{MS}} = 0.04, b_{\text{RG}} = 0.04$], $\mathcal{R}_{\text{Ia}}/\mathcal{R}_{\text{II}} \sim 0.47$ and 0.26 for early and late type spirals, respectively, which are larger than the observed values (Cappellaro et al. 1999). For [$b_{\text{MS}} = 0.01, b_{\text{RG}} = 0.055$], $\mathcal{R}_{\text{Ia}}/\mathcal{R}_{\text{II}} \sim 0.28$ and 0.21 for early and late type spirals, respectively, which are smaller. However, these sets of b parameters may be allowed in view of the possible systematic errors and the inhomogeneity of the samples. We need further updates of the present supernova rates to test our model.

b) *SN Ia rate in elliptical galaxies* — In ellipticals, the star formation has stopped more than 10 Gyr before and only SNe Ia from the RG+WD system occur at present (Fig.5). Thus b_{RG} can be constrained from the present SN Ia rate in ellipticals. For example, if we adopt the sets of [$b_{\text{MS}} = 0.04, b_{\text{RG}} = 0.04$] and [$b_{\text{MS}} = 0.055, b_{\text{RG}} = 0.01$], the predicted SN Ia rates are by a factor of ~ 2 higher and lower than the observed values (Cappellaro et al. 1999), respectively. However, such differences from the observed rates are comparable to the uncertainty stemming from H_0 , so that these sets cannot be precluded until more accurate H_0 is obtained.

Supernova rates at high and intermediate redshifts

The supernova rates at high and intermediate redshifts can also be used to test our SN Ia model. In particular, whether the b parameters are different among the different types of galaxy could be seen from the evolution of the supernova rates with redshift. Observationally, we have found no significant differences in the binary fraction and the iron abundance between ellipticals and spirals. Theoretically, as noted in section 2.1, b may depend on the binary fraction and the iron abundance; especially, the metallicity dependence of b_{RG} is significant. Here we show the results for the cases that b_{RG} is larger only for ellipticals.

Figure 9 shows the cosmic supernova rates for the set of [$b_{\text{MS}} = 0.05, b_{\text{RG}} = 0.02$] in spirals and [$b_{\text{MS}} = 0.05, b_{\text{RG}} = 0.10$] in ellipticals. In this case the contribution of ellipticals to the cosmic SN Ia rate is as large as that of spirals. The redshifts where the SN Ia rates drop are the same as in Figures 6b and 8b. This is because $z_{\text{Ia,e}}$ of ellipticals is determined by the lifetime of SNe Ia (i.e, the time-redshift relation) and not the iron abundance of the galaxy (i.e., the age-metallicity relation, which is effective only for spirals), while the difference in b affects only the latter relation. Whether the contribution of ellipticals is actually as large as spirals will be seen soon in the observations for the intermediate redshifts (B. Schmidt, private communication).

In the above case, the present SN Ia rate in ellipticals is ~ 5 times larger than the observed rate (Cappellaro et al. 1999). However, the SN Ia rate could significantly decrease to the present, if the lowest mass of the RG companions to produce SNe Ia is not $0.9M_{\odot}$ (with the lifetime of ~ 19 Gyr for $Z = 0.02$) but $1.0M_{\odot}$ (with the lifetime of ~ 12 Gyr for $Z = 0.02$), because the star formation in ellipticals has stopped 14 Gyr before in our model. Whether the longest lifetime of SNe Ia is actually younger than the age of ellipticals can be seen from the intermediate redshift observations.

REFERENCES

- Arimoto, N., & Yoshii, Y. 1987, A&A, 173, 23
 Arimoto, N., Yoshii, Y., & Takahara, F., 1992, A&A, 253, 21
 Baugh, C. M., Cole, S., Frenk, C. S., & Lacey, C. G., 1998, ApJ, 498, 504
 Bernardi, M., Renzini, A., da Costa, L. N., Wegner, G., Alonso, M. V., Pellegrini, P. S., Rit e, C., & Willmer, C. N. A. 1998, ApJ, 508, 143
 Branch, D., Livio, M., Yungelson, L. R., Boffi, F. R., & Baron, E. 1995, PASP, 107, 717
 Canizares, C. R., Fabbiano, G., & Trinchieri, G. 1987, ApJ, 312, 503
 Cappellaro, E., Turatto, M., Tsvetkov, D. Yu., Bartunov, O.S., Pollas, C., Evans, R., & Hammuy, M., 1997, A&A, 322, 431
 Cappellaro, E., Evans, R., & Turatto, M. 1997, A&A, 351, 459
 Casoli, F., Sauty, S., Gerin, M., Boselli, A., Fouqu e, P., Braine, J., Gavazzi, G., Lequeux, J., & Dickey, J. 1998, A&A, 331, 451
 Connolly, A. J., Szalay, A. S., Dickinson, M., SubbaRao, M. U., & Brunner, R. J. 1997, ApJ, 486, L11

- de Vaucouleurs, G., de Vaucouleurs, A., Corwin, H.G., Buta, R. J., Paturel, G., & Fouque, P. 1991, *Third Reference Catalogue of Bright Galaxies (RC3)*, (New York: Springer-Verlag)
- Dressler, A., 1980, *ApJ*, 236, 351
- Dressler, A., Oemler, A., Couch, W. J., Smail, I., Ellis, R. S., Barger, A., Butcher, H., Poggianti, B. M., & Sharples, R.M., 1997, *ApJ*, 490, 577
- Duguennoy, A., & Mayor, M. 1991, *A&A*, 248, 485
- Franceschini, A., Silva, L., Fasano, G., Granato, G. L., Bressan, A., Arnouts, S. & Danese, L. 1998, *ApJ*, 506, 600
- Fukugita, M., Hogan, C. J., & Peebles P. J. E. 1998, *ApJ*, 503, 518
- Gallego, J., Zamorand, J., Aragón-Salamanca, A., & Rego, M. 1995, *ApJ*, 455, L1
- Gilliland, R. L., Nugent, P. E., & Phillips, M. M. 1999, *ApJ*, 521, 30
- Glazebrook, K., Blake, C., Economou, F., Lillij S., & Colles, M. 1999, *MNRAS*, 306, 843
- Gratton, R. G., Fusi Pecci, F., Carretta, E., Clementini, G., Corsi, C. E., & Lattanzi, M. 1997, *ApJ*, 491, 749
- Gronwall, C. 1998 (astro-ph/9806240)
- Hachisu, I., & Kato, M., 2000, in preparation
- Hachisu, I., Kato, M., & Nomoto, K. 1996, *ApJ*, 470, L97
- Hachisu, I., Kato, M., & Nomoto, K. 1999b, *ApJ*, 522, 487
- Hachisu, I., Kato, M., Nomoto, K., & Umeda, H. 1999a, *ApJ*, 519, 314
- Harris, W. E. et al. 1997, *AJ*, 114, 1030
- Höflich, P., & Khokhlov, A. 1996, *ApJ*, 457, 500
- Hughes, D., et al. 1998, *Nature*, 394, 241
- Iben, I. Jr., & Tutukov, A. V. 1984, *ApJS*, 54, 335
- Iglesias, C. A., & Rogers, F. 1993, *ApJ*, 412, 752
- Kauffmann, G., & Charlot, S., 1998, *MNRAS*, 294, 705
- Kobayashi, C., & Arimoto, N. 1999, *ApJ*, 527, 573
- Kobayashi, C., Tsujimoto, T., Nomoto, K., Hachisu, I., & Kato, M. 1998, *ApJ*, 503, L155 (K98)
- Kochanek, C. S. 1997, *ApJ*, 491, 13
- Kodama, T., & Arimoto, N., 1997, *A&A*, 320, 41
- Kodama, T., Bower, R. G., & Bell, E. F. 1999, *MNRAS*, 306, 561
- Larson, R. B., 1974, *MNRAS*, 169, 229
- Li, X. -D., & van den Heuvel, E. P. J. 1997, *A&A*, 322, L9
- Lilly, S. J., Le Fèvre, O., Hammer, F., & Crampton, D. 1995, *ApJ*, 460, L1
- Low, C. & Lynden-Bell, D. 1976, *MNRAS*, 176, 367
- Madau, P., Ferguson, H. C., Dickinson, M. E., Giavalisco, M., Steidel, C. C., & Fruchter, A. 1996, *MNRAS*, 283, 1388
- Madau, P., Della Valle, M., & Panagia, N. 1998, *MNRAS*, 297, 17
- Matsushita, K. et al. 1994, *ApJ*, 436, L41
- Nomoto, K., & Kondo, Y. 1991, *ApJ*, 367, L19
- Nomoto, K., Iwamoto, K., & Kishimoto, N. 1997a, *Science*, 276, 1378
- Nomoto, K., Iwamoto, K., Nakasato, N., Thielemann, F.-K., Brachwitz, F., Tsujimoto, T., Kubo, Y., & Kishimoto, N. 1997b, *Nuclear Physics*, A621, 467c
- Nomoto, K., Umeda, H., Hachisu, I., Kako, M., Kobayashi, C., & Tsujimoto, T. 2000 in *Type Ia Supernovae: Theory and Cosmology*, ed. J. Truran & J. Niemeyer (Cambridge: Cambridge University Press), in press (astro-ph/9907386)
- Nomoto, K., Yamaoka, H., Shigeyama, T., Kumagai, S., & Tsujimoto, T. 1994, in *Supernovae, Les Houches Session LIV*, ed. S. A. Bludman et al. (Amsterdam: North-Holland), 199
- Nugent, P., Baron, E., Branch, D., Fisher, A., & Hauschildt, P. H. 1997, *ApJ*, 485, 812
- Pain, R. 1999, talk at the Type Ia Supernova workshop (Aspen Center for Physics)
- Pain, R., et al. 1996, *ApJ*, 473, 356
- Pei, Y. C., & Fall, S. M., 1995, *ApJ*, 454, 69
- Pence, W. 1976, *ApJ*, 420, L1
- Perlmutter, S. et al. 1999, *ApJ*, 517, 565
- Pettini, M., Kellogg, M., Steidel, C. C., Dickinson, M., Adelberger, K. L., & Giavalisco, M. 1998, *ApJ*, 508, 539
- Roberts M. S. & Haynes M. P. 1994, *ARA&A*, 32, 115
- Rowan-Robinson, M., et al. 1997, *MNRAS*, 289, 490
- Ruiz-Lapuente, P., & Canal, R. 1998, *ApJ*, 497, L57
- Sadat, R., Blanchard, A., Guiderdoni, B., & Silk, J. 1998, *A&A*, 331, L69
- Saio, H., & Nomoto, K. 1985, *A&A*, 150, L21
- Saio, H., & Nomoto, K. 1998, *ApJ*, 500, 388
- Salpeter, E. E. 1955, *ApJ*, 121, 161
- Schmidt, M. 1959, *ApJ*, 129, 243
- Schmidt, B. et al. 1998, *ApJ*, 507, 46
- Segretain, L., Chabrier, G., & Mochkovitch, R. 1997, *ApJ*, 481, 355
- Silk, J. 1977, *ApJ*, 214, 718
- Stanford, S. A., Eisenhardt, P. R. M., & Dickinson, M., 1998, *ApJ*, 492, 461
- Steidel, C. C., Adelberger, K.L., Giavalisco, M., Dickinson, M., & Pettini, M. 1999, *ApJ*, 519, 1
- Tinsley, B. M. 1980, *Fundamentals of Cosmic Physics Vol.5*, p.287
- Totani, T., Yoshii, Y., & Sato, K. 1997, *ApJ*, 483, L75
- Tresse, L., & Maddox, S. J. 1998, *ApJ*, 495, 691
- Treyer, M. A., Ellis, R. S., Milliard, B., Donas, J., & Bridges, T. J. 1998, *MNRAS*, 300, 303
- Tsujimoto, T., Nomoto, K., Yoshii, Y., Hashimoto, M., Yanagida, S., & Thielemann, F.-K. 1995, *MNRAS*, 277, 945
- Tsujimoto, T., Yoshii, Y., Nomoto, K., Matteucci, F., Thielemann, F. -K., & Hashimoto, M. 1997, *ApJ*, 483, 228
- Tutukov, A. V., & Yungelson, L. R. 1994, *MNRAS*, 268, 871
- Umeda, H., Nomoto, K., Kobayashi, C., Hachisu, I., & Kato, M. 1999, *ApJ*, 522, L43
- Umeda, H., Nomoto, K., & Nakamura, T. 2000, in *The First Stars*, ed. A. Weiss et al. (Berlin: Springer), in press (astro-ph/9912248)
- Wang, L., Höflich, P., & Wheeler, J. C. 1997, *ApJ*, 483, L29
- Webbink, R. F. 1984, *ApJ*, 277, 355
- Worthey, G., Faver, S. M., & Gonzalez, J. J. 1992, *ApJ*, 398, 69
- Yoshii, Y., Tsujimoto, T., & Nomoto, K. 1996, *ApJ*, 462, 266
- Yungelson, L., & Livio, M. 1998, *ApJ*, 497, 168
- Yungelson, L., & Livio, M. 2000, *ApJ*, 528, 108
- Zepf, S. E. 1997, *Nature*, 390, 27

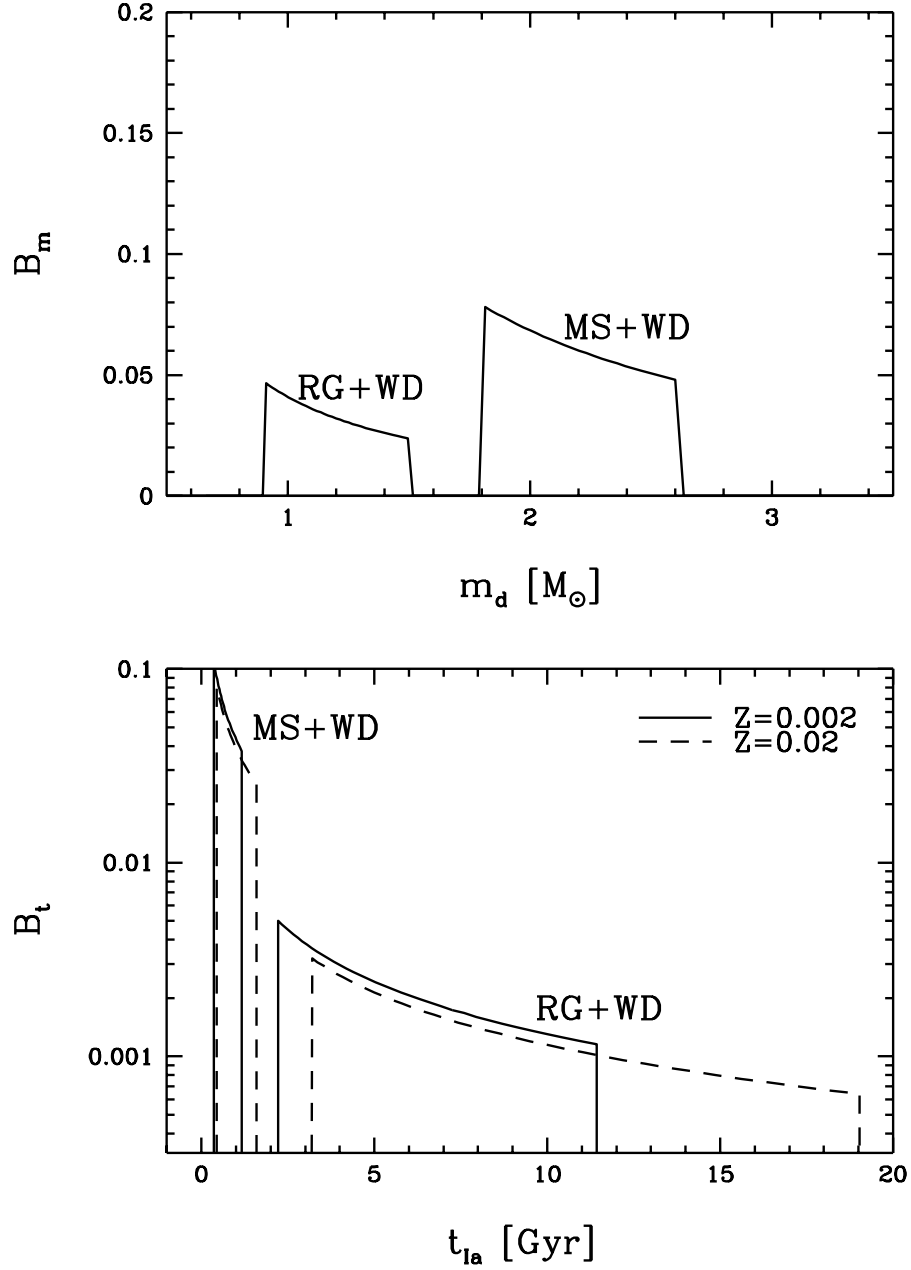


FIG. 1.— The distribution functions of the companion mass (upper panel) and the companion lifetime (lower panel). In the lower panel, the solid and dashed lines are for $Z = 0.002$ and $Z = 0.02$ (solar), respectively. MS+WD and RG+WD denote that the companions of the white dwarfs (WD) is the somewhat evolved near main-sequence (MS) star and the red-giant (RG), respectively.

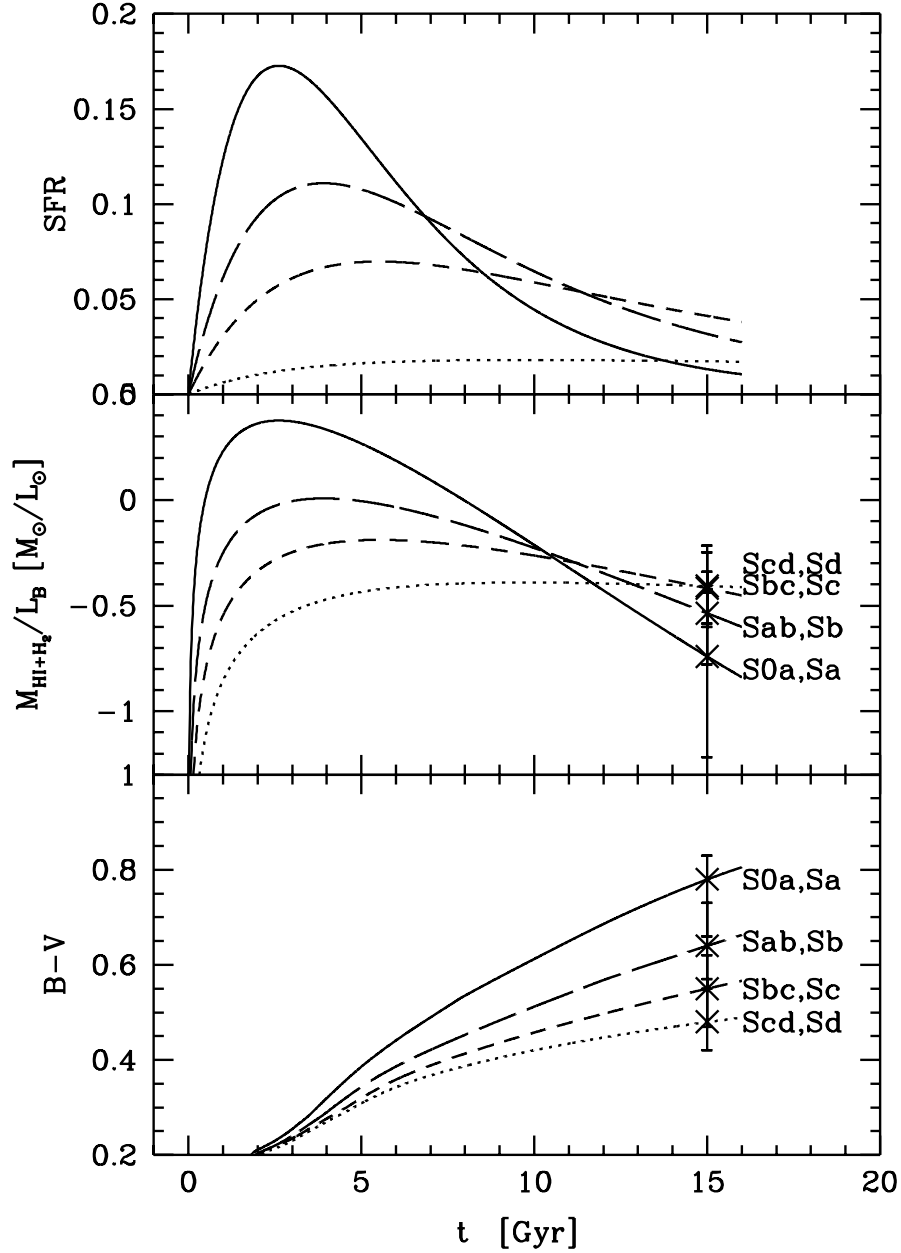


FIG. 2.— Star formation rates (SFR: top panel), gas fractions (middle panel), and $B - V$ colors (bottom panel) as a function of time for four types of spirals : S0a-Sa (solid line), Sab-Sb (long-dashes line), Sbc-Sc (short-dashed line), and Scd-Sd (dotted line). The crosses show the present observed values of colors and gas fractions. The present $B - V$ colors are taken from Roberts & Haynes (1994). We use the gas (i.e., $\text{HI} + \text{H}_2$) fractions which are normalized by the present blue luminosity of the galaxy to avoid the uncertainty in the fractions of the dark matter. The HI mass is taken from Roberts & Haynes (1994), and the H_2 mass is derived from the H_2/HI ratios (Casoli et al. 1998).

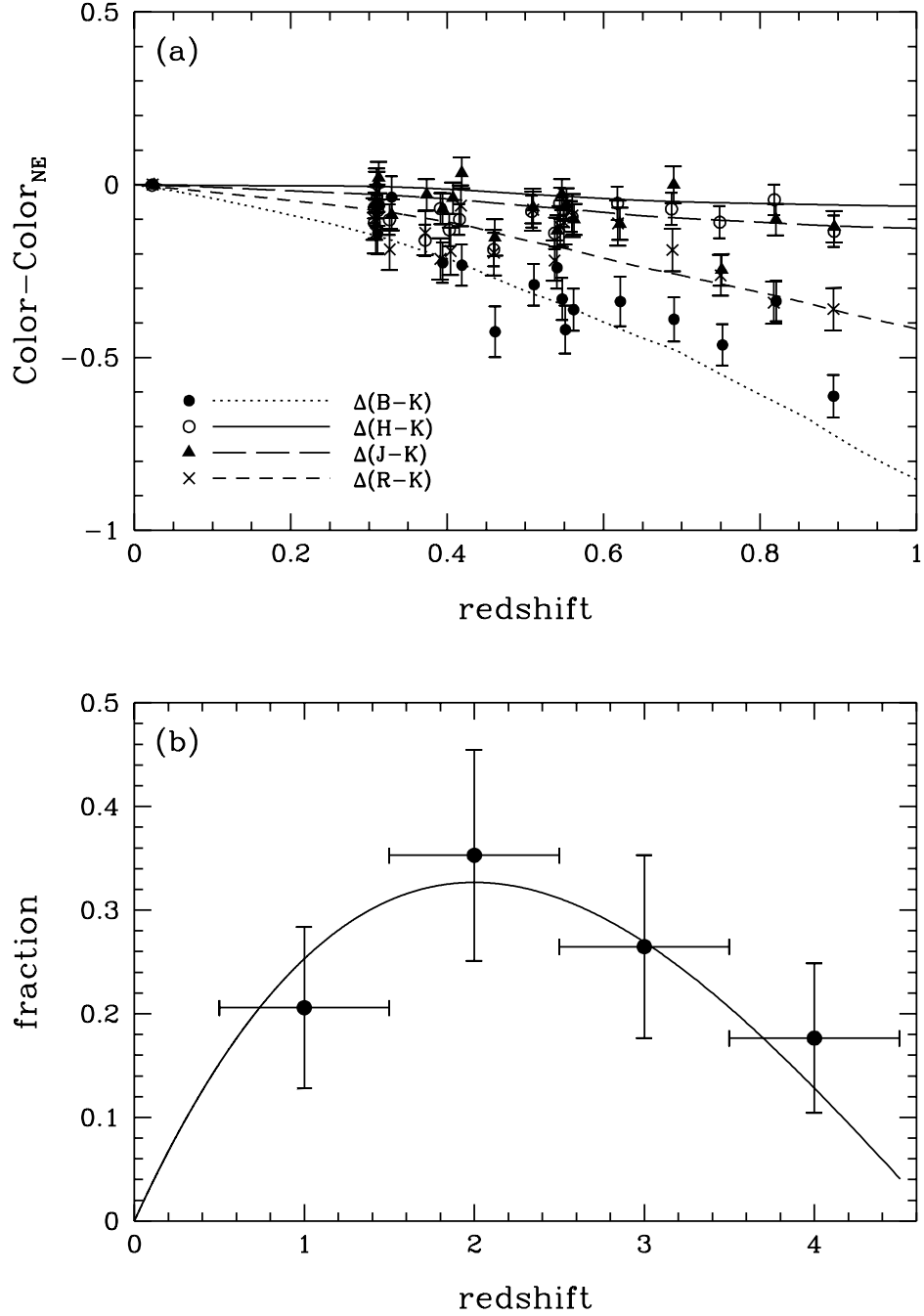


FIG. 3.— (a) The passive color evolution predicted by the model of cluster ellipticals from the present to $z \sim 1$, compared with the observational data (Stanford, Eisenhardt & Dickinson 1998). (b) The distribution function of the formation epoch adopted in the model of field ellipticals. The observational data are estimated from the spectra of ellipticals in the Hubble Deep Field (Franceschini et al. 1998).

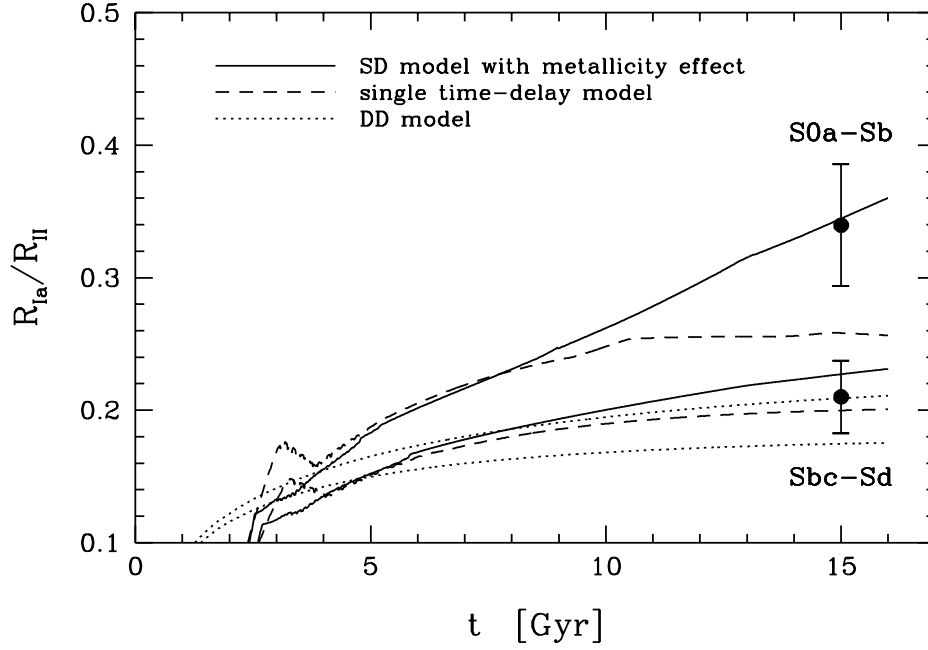


FIG. 4.— The ratio of the SN Ia rate to SN II rate $\mathcal{R}_{Ia}/\mathcal{R}_{II}$ as a function of time for spiral galaxies. The upper and lower lines show the results for the early-type spirals S0a-Sb and for late-type spirals Sbc-Sd, respectively. The solid, dashed, and dotted lines are calculated with our SN Ia model, the single delay-time model with $t_{Ia} \sim 1.5$ Gyr (Yoshii et al. 1996), and the DD model (Tutukov & Yungelson 1994), respectively. The observational data are taken from Cappellaro et al. (1999).

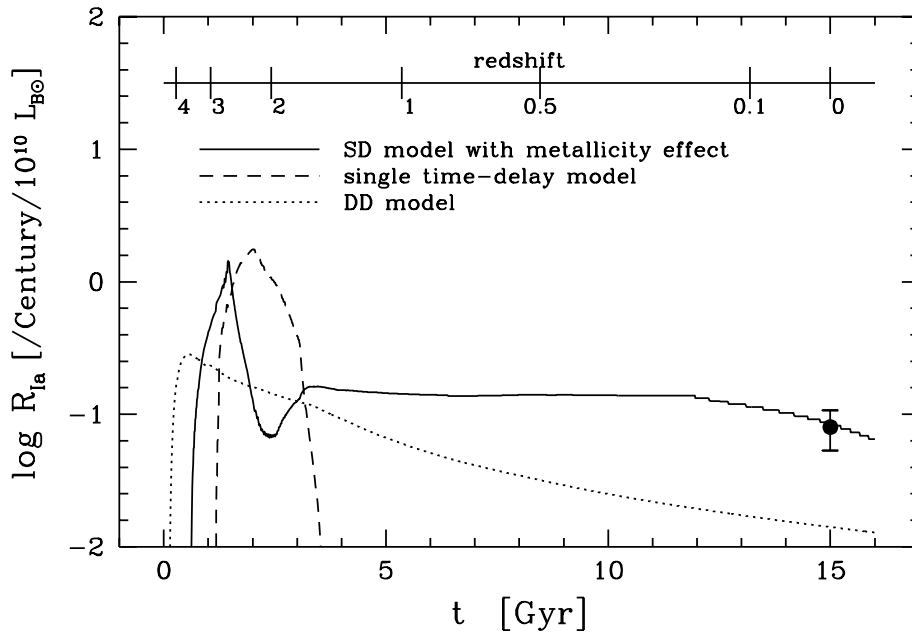


FIG. 5.— The SN Ia rate as a function of time in elliptical galaxies. Lines are the same as in Figure 4. The observational data is taken from Cappellaro et al. (1999).

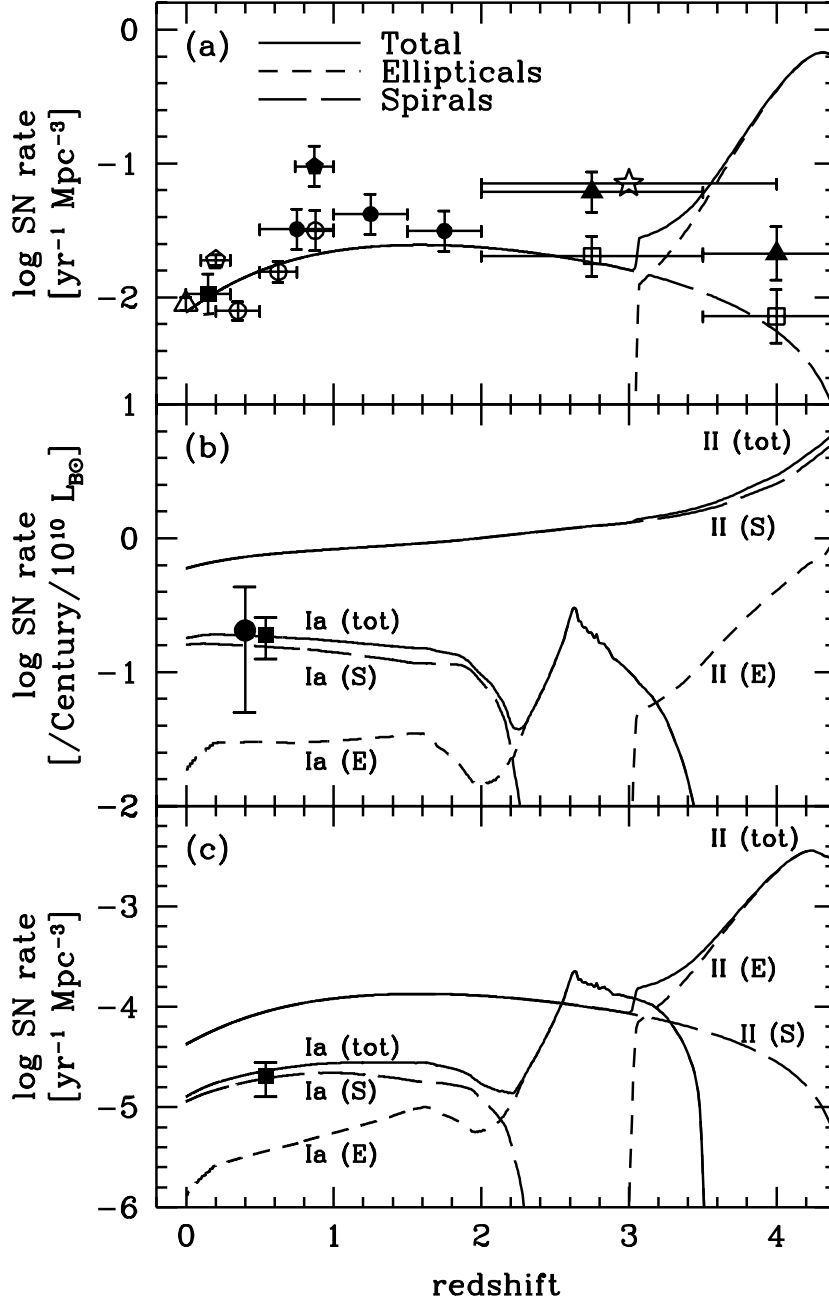


FIG. 6.— (a) The cosmic SFR along redshift (solid line) as a composite of those in spirals (long-dashed line) and ellipticals (short-dashed line). The symbols are the observational data for the cosmic SFR (Gallego et al. 1995, open triangle; Lilly et al. 1996, open circles; Madau et al. 1996, open squares; Connolly et al. 1997, filled circles; Tresse & Maddox 1998, open pentagon; Treyer et al. 1998, filled square; Glazebrook et al. 1999, filled pentagon; Hughes et al. 1998, star; Pettini et al. 1998, filled triangle). (b) The cosmic supernova rate (solid line) as a composite of those in spirals (long-dashed line) and ellipticals (short-dashed line). The observational data for the cosmic SN Ia rate are taken from Pain et al. (1996; circle) and Pain (1999; square). (c) The cosmic supernova rate per volume (solid line) as a composite of those in spirals (long-dashed line) and ellipticals (short-dashed line). The observational data for the cosmic SN Ia rate is taken from Pain (1999).

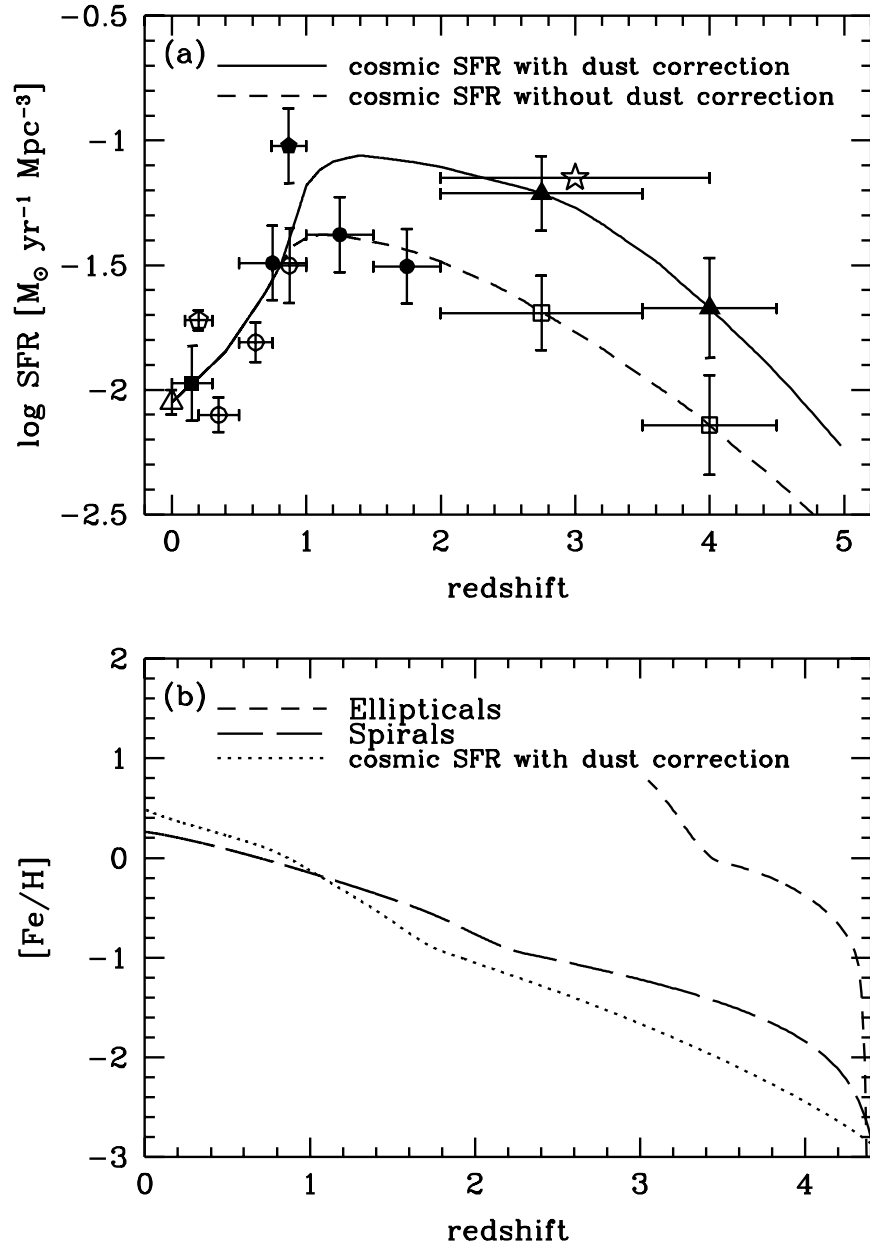


FIG. 7.— (a) The cosmic SFR along redshift which is a connected line of the observed data. The solid line takes into account the correction of the dust extinction (Pettini et al. 1998) and the dotted line does not. (b) The iron abundance in the gas of spirals (long-dashed line) and ellipticals (short-dashed line). For the dotted line, the observed cosmic SFR with the dust correction is adopted.

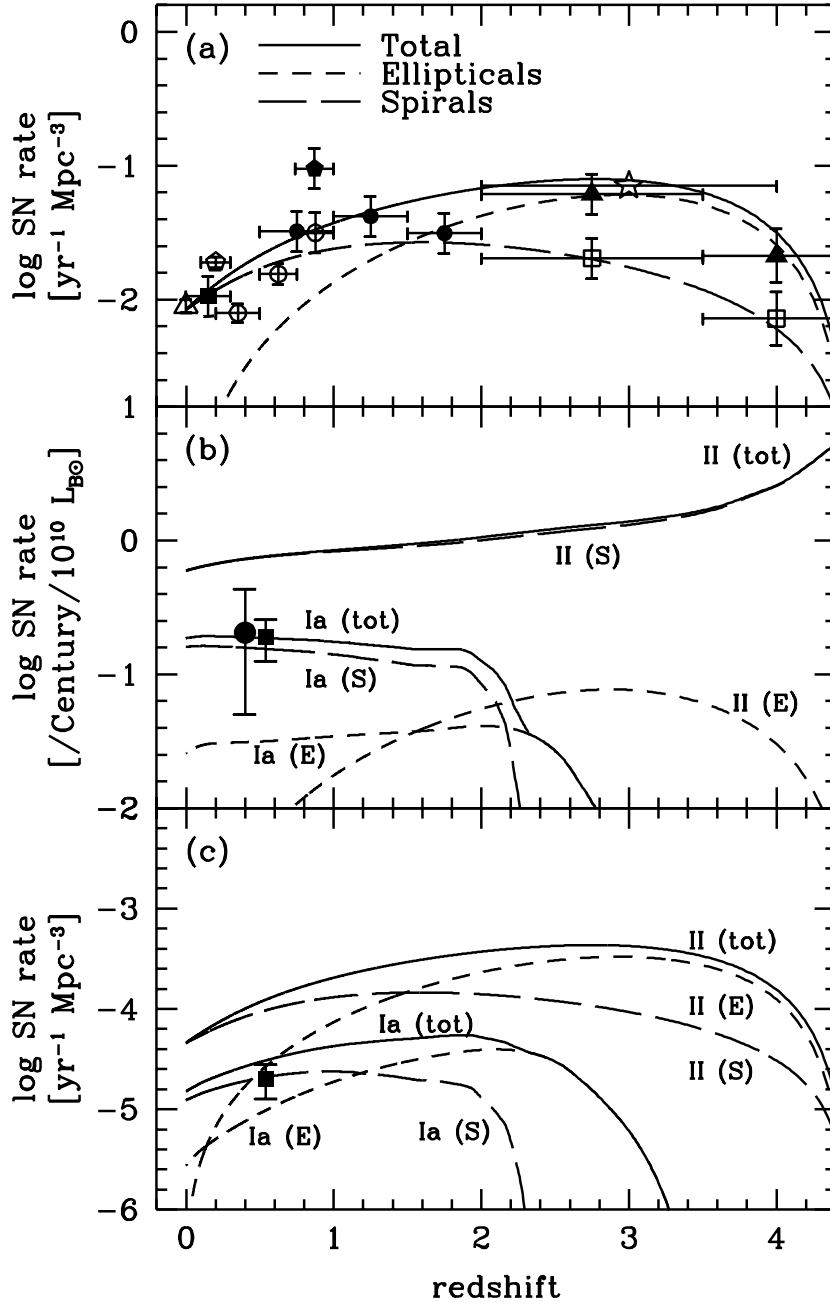


FIG. 8.— The same as Figure 6, but for ellipticals whose formation epochs span over $1 \lesssim z \lesssim 4$; this might correspond to field ellipticals.

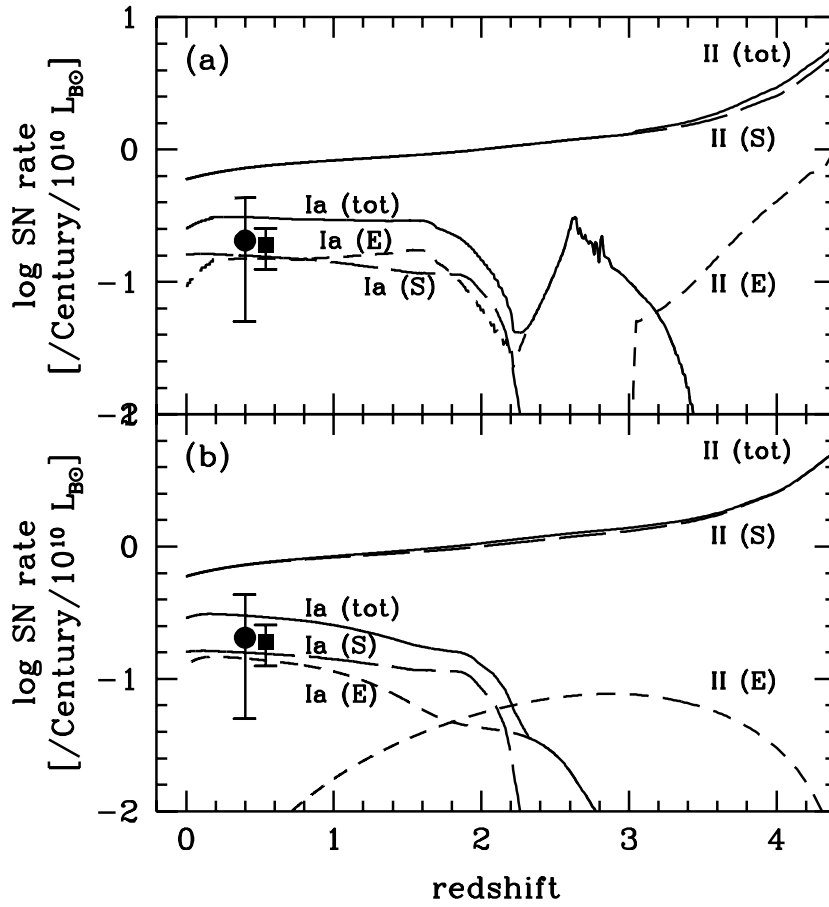


FIG. 9.— The cosmic supernova rate along redshift in clusters (a) and field (b) with $[b_{\text{MS}} = 0.05, b_{\text{RG}} = 0.02]$ for spirals and $[b_{\text{MS}} = 0.05, b_{\text{RG}} = 0.10]$ for ellipticals. Symbols are the same as in Figure 6b.

TABLE 1
THE INPUT PARAMETERS IN EQUATIONS (3) AND (4).

(1)	τ_s [Gyr] (2)	τ_i [Gyr] (3)
E	0.1	0.1
S0a, Sa	2.32	2.35
Sab, Sb	2.19	5.61
Sbc, Sc	2.39	10.92
Scd, Sd	2.19	60.5

Col.(1).—Galaxy type.

Col.(2)(3).—Timescales of the star formation and inflow in Gyr.

TABLE 2
THE CALCULATED QUANTITIES FOR SPIRALS AND ELLIPTICALS AT 15 GYR.

(1)	f_g \mathcal{R}_{II} (2) (10)	f_s \mathcal{R}_{Ia} (3) (11)	$[M/H]_g$ \mathcal{R}_{II} (4) (12)	$[M/H]_s$ \mathcal{R}_{Ia} (5) (13)	$[Fe/H]_g$ $B - V$ (6) (14)	$[Fe/H]_s$ $U - B$ (7) (15)	$[Mg/Fe]_g$ M/L_B (8) (16)	$[Mg/Fe]_s$ M/L_V (9) (17)
E	0.095	0.905	0.176	-0.212	0.831	-0.411	-0.777	0.339
	0.000	0.007	0.000	0.084	0.924	0.339	11.323	8.799
S0a, Sa	0.031	0.968	0.323	-0.160	0.607	-0.026	-0.215	-0.032
	0.072	0.034	0.425	0.198	0.776	0.106	5.880	5.238
Sab, Sb	0.070	0.862	0.082	-0.184	0.315	-0.050	-0.151	-0.032
	0.174	0.051	0.712	0.209	0.631	-0.056	4.105	4.178
Sbc, Sc	0.098	0.648	-0.033	-0.218	0.164	-0.092	-0.109	-0.023
	0.225	0.053	0.853	0.202	0.541	-0.137	3.796	4.199
Scd, Sd	0.038	0.182	-0.124	-0.235	0.051	-0.112	-0.081	-0.019
	0.095	0.019	0.953	0.194	0.472	-0.189	10.085	11.880

Col.(1).— Galaxy types.

Col.(2)(3).— Gas and stellar fractions. For ellipticals, f_g includes the gas ejected in the galactic wind.

Col.(4)(6)(8).— Gas metallicities $[M/H]_g \equiv \log Z/Z_\odot$, iron abundances of gas $[Fe/H]_g$, and magnesium to iron ratios of gas $[Mg/Fe]_g$.

Col.(5)(7)(9).— Mean stellar metallicities $[M/H]_s \equiv \log Z_s/Z_\odot$, mean stellar iron abundances $[Fe/H]_s$, and mean stellar magnesium to iron ratios $[Mg/Fe]_s$.

Col.(10)(11).— SN II and Ia rates per mass in the unit of $[/Gyr/10^3 M_\odot]$.

Col.(12)(13).— SN II and Ia rates per luminosity in the unit of $[/Century/10^{10} L_{B\odot}]$.

Col.(14)(15).— $B - V$ and $U - B$ colors.

Col.(16)(17).— Mass-to light ratios in B- and V-band.